JÖNKÖPING UNIVERSITY
School of Engineering

Licentiate Thesis

The Influence of Microstructure on the Crack Initiation and Propagation in Al-Si Casting Alloys

Toni Bogdanoff

Jönköping University
School of Engineering
Dissertation Series No. 062 • 2021

JÖNKÖPING UNIVERSITY
School of Engineering

Licentiate Thesis

The Influence of Microstructure on the Crack Initiation and Propagation in Al-Si Casting Alloys

Toni Bogdanoff

Jönköping University
School of Engineering
Dissertation Series No. 062 • 2021

Licentiate Thesis in Materials and Manufacturing

The Influence of Microstructure on the Crack Initiation
and Propagation in Al-Si Casting Alloys
Dissertation Series No. 062

Published by
School of Engineering, Jönköping University
P.O. Box 1026
SE-551 11 Jönköping
Tel. +46 36 10 10 00
www.ju.se

Printed by Stema Specialtryck AB 2021

Trycksak
3041 0234

ISBN 978-91-87289-66-8

ABSTRACT

For reducing the CO_2 footprint in many industrial fields, the goal is to produce lighter components. The aluminium-silicon (Al-Si) cast alloys are promising candidates to fulfill these goals with a high weight-to-strength ratio, good corrosion properties, excellent castability, and recyclable material. However, the variations within these components need to be understood to produce high-performance components for critical applications. The main reason for the rejection in these applications is defects and microstructural features that reduce the mechanical properties. The addition of copper (Cu) is one way of increasing the mechanical properties in Al-Si alloys and is commonly used in the automotive industry. Casting defects harm the mechanical properties, and these defects can be reduced by improving the melt quality, the correct design of the component, and the gating system

The study aims to investigate the static mechanical properties and the crack initiation and propagation under cyclic loading in an Al-7Si-Mg cast alloy with state-of-the-art experiments. The main focuses were on the effect of the HIP process and the role of Cu addition. In-situ cyclic testing using a scanning electron microscope coupled with electron back-scattered diffraction, digital image correlation, focused ion beam (FIB) slicing, and computed tomography scanning was used to evaluate the complex interaction between the crack path and the microstructural features.

The amount of Cu retained in the α-Al matrix in as-cast and heat-treated conditions significantly influenced the static mechanical properties by increasing yield strength and ultimate tensile strength with a decrease in elongation. The three-nearest-neighbor distance of eutectic Si and Cu-rich particles and crack tortuosity were new tools to describe the crack propagation in the alloys, showing that a reduced distance between the Cu-rich phases is detrimental for the mechanical properties. Three-dimensional tomography using a FIB revealed that the alloy with 3.2 wt.% Cu had a significantly increased quantity of cracked Si particles and intermetallic phases ahead of the crack tip than the Cu-free alloy. The effect of Cu and HIP process in this work shows the complex interaction between the microstructural features and the mechanical properties, and this needs to be considered to produce high-performance components.

Keywords: Aluminum-Silicon alloys; scanning electron microscopy; material characterization; fatigue performance; digital image correlation;

Sammanfattning

Ett sätt att nå målen med minskade koldioxidutsläpp inom industrin är att producera lättare komponenter. Aluminium-kisel (Al-Si) gjutna legeringar är därför ett bra alternativ då dessa legeringar har ett bra förhållande mellan hållfasthet och vikt, goda korrosionsegenskaper, utmärkt gjutbarhet och är ett återvinningsbart material. En av de största utmaningarna för att producera högpresterande komponenter för kritiska applikationer är variationerna i egenskaper inom dessa komponenter. Orsaken till att inte gjutna Al-Si legeringar andvänds i dessa applikationer är förståelsen av defekter och mikrostruktuella faser påverkar de mekaniska egenskaperna negativt. Koppar (Cu) tillsätts i Al-Si legeringar för att öka de mekaniska egenskaperna vilket ofta nyttjas inom bilindustrin. Hot isostatic pressing (HIP) prosessen är en annan möjlighet att förbättra de mekaniska egenskaperna genom att reducera porositeter i materialet.

Studien syftar till att undersöka de mekaniska egenskaperna och sprickinitiering och spricktillväxt i en gjuten legering av Al-7Si-Mg med utmattningstestning i svepelektronmikroskop (SEM) i kombination med electron backscatter diffraction, digital image correlation och focused ion beam (FIB). Mängden Cu i Al-Si legeringen påverkade de statiska mekaniska egenskaperna genom att öka sträckgränsen och brottgränsen. Tillsats av Cu upp till 1.5 vikt.% påverkar inte spricktillväxten märkbart. Däremot förändras beteendet markant vid tillsatser av Cu på mer än 3.0 vikt.% som resulterade i en markant reducering i duktilitet. I det värmebehandlade materialet påverkades de mekaniska egenskaperna av Al-matrisen och mängden intermetalliska faser. Avståndet mellan Cu faserna och Si faserna används för att beskriva spricktillväxten i Al-Si legeringarna. Detta tillsammans med tredimensionell tomografi visade att legeringen med 3.2 vikt.% Cu hade en ökad mängd sprickor i området framför den avancerande sprickan, vilket inte den Cu fria legeringen visade. Al-Si legeringen som utsattes för HIP-processen och värmebehandlingen visade att materialets mikrostruktur i gjutet tillstånd påverkade resultatet. HIP processen slöt porositerena i alla undersökta prover och förbättrade de mekaniska egenskaperna.

Dessa resultat kommer kunna användas för att konstruera mer högpresterande komponenter.

ACKNOWLEDGEMENTS

I would like to express my sincere gratitude to many people who have supported me along the way:

My main supervisor, Professor Salem Seifeddine, for guidance, support, valuable and criticizing comments, input, and fruitful discussions.

My supervisors, Associate Professor Ehsan Ghassemali, Professor Anders E.W Jarfors, for the support, comments, and advice during the work.

I would like to thank my co-authors, Mattia Merlin and Lucia Lattanzi, for the cooperation and good collaboration.

The technicians, Esbjörn Ollas, Peter Gunnarsson, Jacob Steggo, and Jörgen Bloom, for the assistance with the exprimental work.

All colleagues and friends at the Materials and Manufacturing department for exciting discussions, laughs, and a fantastic working environment.

I am grateful to the people at Unnaryd Modell AB and IAC Ankarsrum AB, and Quintus Technologies AB to produce and test materials.

Thanks to my supporting wife and children for being there.

Toni Bogdanoff

Jönköping 2021

SUPPLEMENTS

The following supplements constitute the basis of this thesis:

Supplement I Bogdanoff, T., Lattanzi, L., Merlin, M., Ghassemali, E., & Seifeddine, S. (2020). The influence of copper addition on crack initiation and propagation in an Al–Si–Mg alloy during cyclic testing. *Materialia*, *12*, 100787.

Toni Bogdanoff was the main author, T. Bogdanoff and L. Lattanzi performed the experimental work together, M, Merlin, E, Ghassemali and S, Seifeddine contributed with advice throughout the work and revising the manuscript.

Supplement II Bogdanoff, T., Lattanzi, L., Merlin, M., Ghassemali, E., Jarfors, A, & Seifeddine, S. (2021) The complex interaction between the microstructure features on the crack initiation and propagation in heat-treated Al-Si-Mg-Cu alloys. Submitted to the Materials Science and Engineering: A, under review.

Toni Bogdanoff was the main author, T. Bogdanoff and L. Lattanzi performed the experimental work together, M, Merlin, E, Ghassemali, A, Jarfors and S, Seifeddine contributed with advice throughout the work and revising the manuscript.

Supplement III Bogdanoff, T., Ghassemali, E., Jarfors, A, & Seifeddine, S. (2021) The impact of HIP process and heat treatment on the fatigue performance of an Al-Si-Mg alloy component. Manuscript, to be submitted to LMT conference.

Toni Bogdanoff was the main author, T. Bogdanoff performed the experimental. E, Ghassemali, A, Jarfors and S, Seifeddine contributed with advice throughout the work and revising the manuscript.

TABLE OF CONTENTS

CHAPTER 1

INTRODUCTION

CHAPTER INTRODUCTION

This chapter describes the background to this work, an introduction to the aluminium-silicon (Al-Si) cast alloys, the influence of alloying elements, pre-and post-treatment effect on the microstructure and mechanical properties. The microstructure features that influence crack initiation and propagation are described.

1.1 BACKGROUND

The strive to reduce greenhouse gas emissions is becoming more critical in the last centuries with legislation and laws to reduce carbon dioxide (CO_2) emissions. These CO_2 emissions have a significant effect on global warming, which leads to the Paris Agreement to reduce greenhouse gas emissions by at least 40 % by 2030 compared to 1990's emissions. The automotive sector is forced to lower the CO_2 emissions either with more efficient engines, reduced weight throughout light-weight materials, or new power sources for vehicles like electrical or hydrogen. The constant growth in the importance of aluminium (Al) usage is directly related to mass reduction because several beneficial properties make it a vital material choice for engineering solutions [1, 2]. Al is used in wrought and cast alloys, which are a light-weight option because of their high strength-to-weight ratio and manufacturing cost efficiency. Moreover, the recyclability of Al uses less energy than the production of primary Al, with savings of up to 95 % in the production of recycled Al alloys [3]. Serrenho et al. [1] show the importance of light-weight in electric cars by 2050, suggesting that the weight reduction could produce the most significant emission saving, and proposed Al as a valid candidate.

Despite all potential applications for Al alloys, fatigue performance in high-cycle fatigue (HCF) has always been controversial since 90 % of all failures are related to fatigue [4]. In cast material, the HCF lifetime reduces drastically when defects such as oxide, pores, and surface roughness are present at surface or subsurface level [5]. Nyahumwa et al. [6] presented that the fatigue life in Al castings may only reach 1 % of their potential because of defects. However, producing a cast material with a low amount of defects or using mechanical treatment to minimize these

defects will improve fatigue life, and the intrinsic material properties are becoming essential.
Pure Al has low strength and is rarely used in engineering applications, and has to be alloyed to achieve the desired properties. These additions of alloying elements determine the mechanical, chemical, and physical properties of the alloy. The addition of copper (Cu) and magnesium (Mg) in Al-Si alloys often used in the automotive industry to increase the mechanical properties due to the solid solution and precipitation strengthening [7-12]. The morphology, size, and distribution of microstructural features affect the mechanical properties of these Al-Si alloys. It is well accepted that a refined microstructure enhances the mechanical properties, which can be achieved with chemical modification or rapid cooling rate [13].

1.2 History

Aluminium (Al) is the third most abundant element in the earth's crust (8%), and only iron is more industrially used [3]. Al is a relatively new material compared to other metals such as iron, copper, tin, etc. In 1825 was pure Al first developed on a small scale. However, the first factory production started in the 1850s, whereas chemical Al was produced more expensive than gold. The revolutionary economically viable production was developed independently by Hall and Heroult in 1886 by electrolysis of alumina (Al_2O_3) dissolved in cryolite (Na_3AlF_6) [3, 14]. The last step to reach high Al production was the production of alumina from bauxite ore around the 1890s. However, the primary Al produced is energy-intensive, and the plants are beneficial places where the electricity cost is low [14]. However, a critical benefit for a sustainable society is the recycling of Al, which only requires 5 % of the energy to produce primary Al [15].

1.3 Aluminium

After the start of large production of Al has the interest in the material increased because of the high weight-to-strength ratio, high corrosion resistance, thermal and electrical properties, and recyclability.

There are two main categories of aluminium:

- Wrought aluminium is the largest category, and it consists of the casting of ingots or billets for either hot or cold forming to produce parts. Extrusion, forging, and rolling are standard manufacturing techniques.

- Cast aluminium, where the melt is poured into a mold made from either steel, sand, plaster, etc., to produce the final shape that can be a complex near-net shaped part with accurate dimensions.

The castability is the most significant difference between the wrought and cast alloys [16].

1.3.1 Al-Si alloys

Among the Al foundry alloys, the Al-Si family is the most used cast alloy because of its excellent castability, high strength to weight ratio, and moderate cost. The commercial Al-Si alloys have Silicon (Si) concentrations between 5 - 23 wt.%, leading to a wide range of applications.
The Al-Si phase diagram in Figure 1 reveals that the eutectic point is at 12.6 wt. % Si and the eutectic temperature is 577 °C, the solubility of Si in Al is ~ 1.65 wt. %.

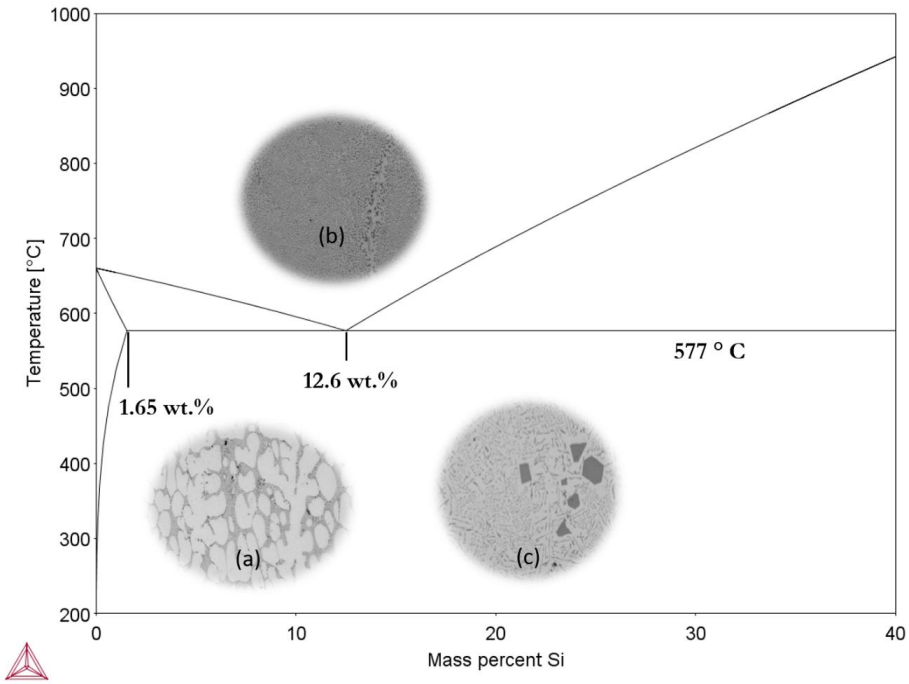

Figure 1. Al-Si phase diagram, a) hypoeutectic, b) eutectic, c) hypereutectic microstructure

The Al-Si alloys are divided into three different families depending on the Si concentration: hypoeutectic, eutectic, and hypereutectic alloys. The hypoeutectic alloy below 12.6 wt.% Si consists of the α-Al matrix and interdendritic Al-Si eutectic, widely used in the automotive sector [15, 17]. Primary Si particles and Al-Si eutectic are the constituents of the hypereutectic alloys with Si concentration above 12.6 wt.%, that are showing excellent wear properties and used in, for example, piston and cylinder liners [18]. The addition of other elements to the Al-Si system or changing the solidification rate may shift the temperatures and eutectic composition, etc. [19, 20].

Si is one of the elements added that reduces the density, improves the fluidity, and decreases the solidification shrinkage. Furthermore, this results in an increased castability. Si also increases both strength and hardness of the material caused by a load transfer from the α-Al matrix to the interconnected eutectic Si plates network [21].

Furthermore, these eutectic Si particles can be modified or spherodized, which reduces the load transfer resulting in improved ductility and fatigue performance [22].

The α-Al matrix phase is comprised of dendritic grains that usually contain several secondary dendrite arms. The size of these secondary dendrite arms is commonly used as a measurement referred to as secondary dendrite arm spacing (SDAS). The SDAS is an important microstructure measurement in castings because it is related to the cooling rate. With higher cooling rates, the dendrite size, particle size, and defects become smaller, generally improving the properties of the alloy. The SDAS and cooling rate relationship is shown in equation 1:

$$SDAS = K * CR^{n} \quad (1)$$

Whereas CR is the cooling rate (°C/s), and K and n are material constants [23].

1.3.2 Alloying element

In Al-Si alloys, alloying elements are added to modify the properties, for example, castability, strength, wear resistance, etc. The main alloying elements are Si, Mg, Cu, and iron (Fe).

The addition of Cu increases the strength of the alloy, with a reduction in ductility [24]. This compromise between strength and ductility is affected by several factors such as; (1) if the Cu is present as phases formed during solidification, (2) or as atoms are in solid solution, (3) or as precipitates after aging [25]. The Cu addition is usually in the range of 0.5 wt % to 3 wt.% [9]. When Cu is retained as atoms in solid solution in the α-Al matrix, it provides the best combination of strength and

ductility at room temperature. Moreover, the addition of Cu reduces corrosion resistance [8].

The addition of Mg improves the strength in as-cast and heat-treated conditions. Addition in the range up to 0.6 wt.% leads to higher corrosion resistance and good machinability at the expense of castability [26]. Moreover, the addition of magnesium in the alloy could form MgO and spinel ($MgAl_2O_4$) oxides that are detrimental to the properties [27].

Fe is always present in cast Al-Si alloys and can be identified as an alloying element or impurity. The presence of Fe is detrimental to the mechanical properties and castability but necessary for high pressure die casting to prolong the lifetime of the tool because of the reduction in die soldering. The Fe solubility in Al is ~0.04 wt.% at 655 °C, leading to Fe intermetallics formation. α-Al_8Fe_2Si, β-Al_5FeSi, and π-$Al_9FeMg_3Si_5$ are the Fe phases that commonly form in Al-Si alloys [28]. These phases are different in morphology, whereas the β-Al_5FeSi are the most detrimental because of the complex 3-dimensional structures observed as a needle in 2-dimensional [29]. The addition of various elements such as chromium, manganese, and nickel are usually used to suppress the formation of β-Al_5FeSi [28, 30].

Strontium (Sr) and sodium (Na) addition promotes the modification of the eutectic Si from an interconnected Si plate network into a fibrous morphology [31].

Titanium (Ti) and boron (B) addition promote grain refinement in Al-Si alloys [32].

1.4 Solidification

Solidification is a phase transformation from liquid to solid. The solidification is crucial to understand the mechanical performance of the component in different conditions. Whereas clusters of atoms form in the liquid at temperatures higher than the start of solidification, they are not stable and dissolve. The melt needs to have a driving force, in this case undercooling, to form a stable nucleus to start the growth of the α-Al dendrites. The growth of the α-Al dendrites continues as the temperature reaches the Al-Si reaction [33].
The commercial Al-Si alloys usually contain alloying elements such as Cu and Mg and impurities such as Fe. These alloying elements nucleate and grow intermetallic phases during the solidification sequence. Cu and Mg intermetallics usually occur after the Al-Si eutectic while the Fe phases could appear before the Al-Si eutectic [34].

During solidification of the Al-Si-Mg alloys, up to 0.6 wt % Mg, the β-Mg2Si and π-$Al_8FeMg_3Si_6$ phases form because of the non-equilibrium solidification condition of the casting process. However, in Al-Si-Mg-Cu, the concentration of Cu changes the solidification sequence in the material where the θ-Al_2Cu phases are formed either as blocky or fin eutectic at low Cu concentrations.
Above 1 wt.% Cu, the Q-$Al_5Mg_8Cu_2Si_6$ phases and θ-Al_2Cu also formed together, suppressing the β-Mg_2Si phase [11, 35-37]. The size and distribution of the intermetallic phases affect the ductility of the alloy. Moreover, the addition of Cu to Al-Si-Mg also influences melt quality, porosity, and hot tearing effects, affecting the mechanical properties [7-9].

1.4.1 Imperfections in cast aluminium

Imperfections in cast aluminium are the reason for most of the premature failure in cast components. These imperfections could be oxides, porosities, intermetallic phases, inclusions, etc., whereas most are referred to as defects. Defects in castings are unwanted and result in reduced strength and elongation to failure with a wider scatter in the properties. The focus of this work is the effect of porosities and oxide films on fatigue properties. The amount of defect depends on the melt quality, pre-treatments to the melt, solidification rate, casting geometry, and casting process. Moreover, the melt quality before casting is affected by the condition of the start material and defects formed during the melt operations. The Al alloys oxidize rapidly in contact with air and forming an oxide film (Al_2O_3) on the melt surface. The oxide film on the melt surface continues to grow in contact with air, but the growth rate decreases as the thickness of the oxide increase. The oxide layer also works as a barrier that reduces the hydrogen into the melt [38]. The transport of the melt between furnaces or during casting may cause turbulence creating entrained folded oxide films see Figure 2.

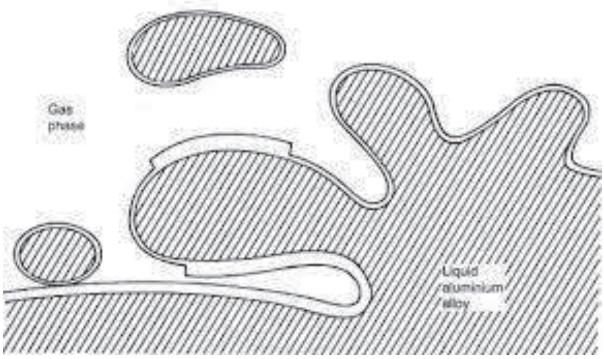

Figure 2. Entrainment of surface oxides [38].

These entrapped oxides from the turbulence in the melt contain two oxide surfaces, usually referred to as bifilms. These bifilms are detrimental to mechanical properties [38-40]. In the filling process, these folded films could follow the melt into the cavity of the component and act as nucleation sites for porosity and Fe-rich intermetallics [41, 42].

Another factor is that the melt has a high solubility of hydrogen in the liquid state see Figure 3. As the melt solidifies, the hydrogen content increase in the remaining liquid that could form porosity if the entrapped hydrogen remains within the casting [39, 43].

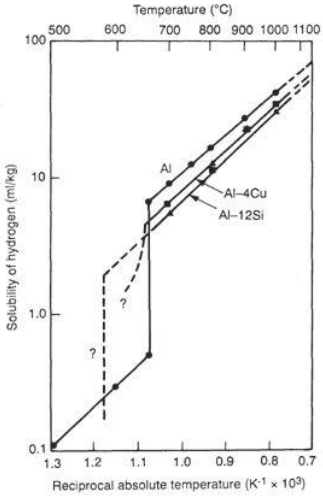

Figure 3. Hydrogen solubility in pure aluminum and two aluminum alloys [38].

The porosity formation comes mainly from the combination of dissolve hydrogen and shrinkage from the solidification process. The literature results generally state that an increased porosity level negatively affects the mechanical properties [44-46]. Moreover, certain alloying elements are reported to increase the porosity content, such as Cu and Sr [10, 47, 48]. To reduce the number of imperfections in cast Al-alloys, pre-treatment to the melt such as degassing could be performed. Degassing reduces the amount of entrapped gas in the melt by introducing gas (usually nitrogen) to the melt, which collects gas and oxides as they float to the surface [41].

1.4.2 Grain refinement

In a cast component, the grains can be either columnar or equiaxed, depending on several parameters such as: alloy composition, thermal gradient, and potent nucleant particles. In Al alloys, fine grain sizes are desired and commonly achieved in the Al industry with the additions of grain refiners. The grain refinement is added using master alloys containing nucleant particles. These master alloys based on the Al-Ti-B system are the most commonly used in the foundry industry. However, foundry alloys are more difficult to grain refine than wrought alloys due to the higher concentration of alloying elements. These nucleant particles promote the formation of an equiaxed microstructure with a uniform distribution of small grains and distribute the porosity, leading to improved mechanical and fatigue properties [32]. The grain refiners are added into the melt before casting to introduce TiB_2 and Al_3Ti particles to the melt, which act as heterogeneously nuclei for the primary Al. The master alloy melts rapidly, and the Al_3Ti dissolves. The refiner particles should ideally be homogeneously distributed in the melt, promoting as many nucleation events on the TiB_2 particles when the solidification starts. However, the density of the TiB_2 particles (~4.5 g/cm^3) is significantly higher than the Al-Si melt that promotes settling if the melt remains stagnant after the addition of grain refiner [32, 49].

The two main groups have been proposed to explain the grain refiner mechanism, classified as the nucleant paradigm and the solute paradigm. Theories concerning only the heterogeneous nucleation mechanism on a nucleant particle are the particle theory [32]. However, segregating elements in the melt affects grain refinement efficiency, leading to the solute paradigm that quantifies the restricting role of segregating elements on the grain refinement. The nuleant particles and the segregating elements have an essential role in grain refinement. The solute paradigm takes the effect of the segregating elements during solidification into account. Easton and StJohn [50] suggested that both solute element and nucleant

particles are needed for grain refinement. StJohn [51] later proposed the interdependence theory, whereas the nucleation event that occurs on the potent particles in front of the growing interface depends on the constitutional undercooling and distance to the next potent particles.

1.4.3Modification

The eutectic modification aims to obtain a change in the Si morphology from flakes to a fibrous structure. The Si modification affects the properties, especially elongation, since the flakes act as stress concentrations sites exposed to loading. However, the load transfer from the α-Al matrix to the interconnected eutectic Si plates network decrease with the fibrous structure. There are different ways to achieve the modification, such as chemical modification and quench modification. Adding modifying elements (Sr, Na, etc.) to the melt at low concentration levels to achieve a chemical modification effect, while a rapid solidification produces a quench modification effect [22]. Several theories have been proposed during the last century, with some theories well-accepted today: the impurity-induced twinning (IIT) introduced by Lu and Hellawell [52] and the restricted twin plan reentrant edge (TPRE) poisoning theory [53].

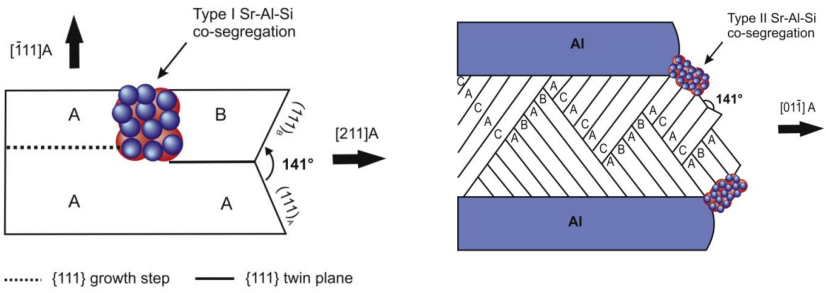

(a) (b)

Figure 4. a) Impurity induced twinning, b) Restricted TPRE growth [54].

These theories state that modifier atoms hinder the anisotropic growth of the Si particle in the [211] direction. In the IIT, the chemical modifiers atoms absorb onto the surface steps restricting the growth and change the growth direction with the formation of new twins see Figure 4a. The restricted TPRE poisons the edges with the modifier atoms. This poisoning effect hinders the growth in the favored [112] direction resulting in isotropic fibrous growth with the branching of the Si particles

see Figure 4b. Timpel et al. [54] showed with atom probe tomography that enrichments of Al and Sr atoms are present inside the Si particles in different segregations types that contribute to the branching of Si particles which confirms that the theories presented above are valid.
Moreover, Lu and Hellawell [52] suggested that the size of the impurity atom plays a crucial role in generating the twin formation. The atomic ratio between the impurity atom and the Si to achieve the best modification should be equal to or greater than 1.65 [52, 54, 55]. The most commonly used modifiers Sr, Na, and Ca, in the foundry industry have an atomic ratio close to the proposed value. However, other modifying elements with an atomic ratio in this range, such as ytterbium and other lanthanides, do not provide an acceptable modification of the Si particles [55].

1.5 Post treatments

1.5.1 Hot isostatic pressing

Hot isostatic pressing (HIP) started as a technique for the diffusion bonding of fuel elements for the nuclear industry [56]. The HIP process has steadily grown from research to a proven manufacturing tool. Moreover, the development of the HIP process equipment made this change possible with a wide range of new applications, such as: upgrading castings, consolidation powders, densifying pre-sintered components, and interfacial bondings [57]. The HIP process has increased from the nuclear industry to several sectors: aerospace, energy, offshore, automotive, and medical. The isostatic pressure in the HIP process originates from gas atoms colliding with the surface of the object. In the process, under particular conditions, the atoms could move with velocities up to 900 m/s, and 10^{30} collision event occurs per square meter per second. These events act on the component, which creates the same pressure in a direction normal to the surface that produces a plastic flow [58]. These plastic flow and diffusion mechanisms help to collapse and shrink internal pores [59]. Manufacturers for critical fatigue applications are generally hesitant to use Al-Si casting due to variations in mechanical properties and quality. The main factor that governs the quality is the shape, distribution, and volume of porosity. However, the HIP process has shown great potential in improving the properties.
Lei et al. [60] studied the effect of the HIP process on the mechanical properties of A356 cast alloys. They observed that the porosity content of HIPped specimens was much less than that of non-HIPped specimens. More than 95 % of porosities were closed by the HIP process. The result showed that the HIP process enhanced fatigue resistance. Moreover, results showed that the HIP process did not significantly

improve the yield strength (YS) and ultimate tensile strength (UTS). Furthermore, in the high cycle fatigue testing, the crack nucleation in the non-HIPped samples started in the large porosity, and the HIPped sampled showed up to a 50 % increase in fatigue strength. Ran et al. [61] reported similar results on unmodified A356 in as-cast and T6 heat-treated conditions. The result is a remarkable decrease in porosity, which is reducing the scatter in the mechanical properties, which showed a significant increase in the UTS and elongation to failure. Ceschini et al. [62] analyzed sand-cast A356 and A204 alloys in HIPped and as-cast conditions. The pore-free castings from the HIP process improved the fatigue strength by 40 and 70 %, respectively.

Brummer et al. [63] investigated an A356 alloy with heat treatment, HIP process, and a combination using HIP process quenching and artificial aging. The result showed that using HIP process and heat treatment, a significant improvement in properties was achieved. The quenching rate was not sufficient in the combined HIP process and aging.

Nyahumwa et al. [6] investigated the casting filling technique and HIP process in an A356 alloy. The result describes that a well-designed bottom gating system could produce reliable Al castings without the HIP process. However, a significant improvement in fatigue life after the HIP process was because of deactivating oxide-film defects. Moreover, the HIP process can heal porosity, but the thicker spinel oxides remain detrimental. Rich et al. [64] investigated two different Al alloys exposed to the HIP process. The results showed improved UTS and elongation to failure. Moreover, the investigation showed an increase in service life in fatigue crack initiation, but no change in the fatigue crack growth rate. The work above shows discrepancy, with some literature showing improved properties while others report a limited impact of the HIP process. Furthermore, the influence within a cast component with different thicknesses on the crack initiation and propagation is crucial for optimizing the performance.

1.5.2 Heat treatment

The general term heat treatment consists of controlled heating and cooling sequences to modify the material properties because of the microstructural changes. The heat treatment objectives are to expand the usage of Al-Si alloys in different industrial applications [65-67]. The T6 heat treatment is one of the most utilized for cast alloys, which consists of three different steps: (1) solution treatment, (2) quenching, and (3) artificial aging, and it is typical for Al-Si-Mg and Al-Si-Cu-Mg alloys [25]. The solution treatment parameters time and temperature depend on the microstructure coarseness and intermetallic phases. Higher solution temperature gives a higher solubility of atoms in the α-Al matrix and a faster time for dissolution,

homogenization, and spheroidization of phases. Increasing the temperature close to the melting point of phases in the alloy could lead to incipient melting, which is detrimental to the mechanical properties [68]. Al-Si-Mg alloys can be solution treated up to 530 °C while the Al-Si-Cu-Mg alloys need to consider what Cu-rich phases form during solidification, such as Q-$Al_5Mg_8Cu_2Si_6$, and θ-Al_2Cu phases. The Q-phase starts to melt at 505 °C, and the solution temperature is commonly set to 495 °C [69].

When the solution treatment cycle is completed, quenching the material at a sufficiently high rate occurs to retrain the soluble atoms in a solid solution. However, if the quenching rate is too low, the precipitation of secondary phases or precipitates starts, which decreases the impact of the heat treatment [70].

The next step after quenching is aging, which can be natural or artificial aging or a combination of both. Natural aging is beneficial for Al-Si-Mg alloys since clusters of atoms form during quenching continue to grow or dissolve depending on their size. It promotes a microstructure with a lower number density of coarser particles than the quenched material [25, 71]. The artificial aging temperature and time are the two parameters used to control the properties of the heat-treated component. At elevated temperatures in the range of 150-210 °C, Guinier-Preston zones start to form the atoms in solid solution, followed by the formation of coherent metastable precipitates. The precipitates continue to grow in size by diffusion of atoms from the solid solution and are semi-coherent with the α-Al matrix. Further growth continues until the precipitate is non-coherent with the α-Al matrix, and last, it forms the non-coherent equilibrium phase [25, 65].

1.6 Mechanical properties

The mechanical properties deviate from the calculated theoretical properties because of inherent metallurgical factors within the material. These factors are imperfections that vary in scale from the atomic scale up to the macro scale and affect the properties differently. On the atomic scale, there are crystallographic imperfections such as dislocations, stacking faults, whereas, on the macro scale, there are imperfections, intermetallics, oxides, and porosity [72].

The static mechanical properties are usually presented with a stress-strain curve, whereas parameters such as YS, young's modulus, UTS, and elongation to failure are evaluated see Figure 5.

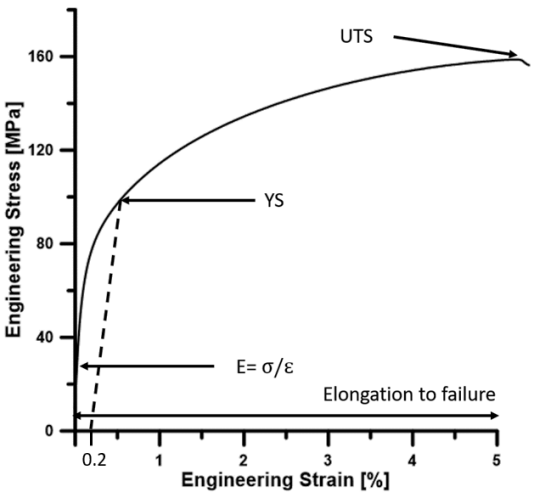

Figure 5. Stress-strain curve of an Al7Si0.3Mg alloy in the as-cast condition. Essential parameters used in the study are highlighted.

The elastic part is the initial linear part of the curve that determines the young´s modulus of the material. The YS is the point where the material starts to plasticize. However, this point is difficult to determine in Al-Si alloys, leading to the usage of a Rp 0.2 offset for the YS. When the load increase above the elastic region, permanent deformation occurs by the motion of dislocation. Obstacles hinder the dislocation motion, such as precipitates, grain boundaries, atoms in solid solution, particles, etc., strengthening the material.

The as-cast material of a cast hypoeutectic Al-Si alloy is characterized by a soft deformable α-Al matrix with low strength surrounded by an Al-Si eutectic network. Together with alloying elements, the Si particles distribution, and shape, imperfections, etc., are the properties influenced [21, 73]. Ghassemali et al. [74] showed that the grain size had a limited influence on the static properties in an Al-Si alloy, while the SDAS showed a significant influence. Several studies of as-cast Al-Si-Mg alloys to which the addition of Cu showed discrepancies in the results due to the fact that the increases in YS and UTS were not of similar magnitude for the same Cu contents. It is worth noting that these results are not directly comparable, as microstructural features such as SDAS and average grain size (AGS) were not clearly stated. Furthermore, pre-treatment to the alloys were not similar such as grain refinement and Sr-modification level [7-9, 11].

One common way to increase the properties in Al-Si alloys with the addition of Cu and Mg is to apply heat treatment to the material, resulting in increased YS and UTS

to the expense of elongation to failure. The increased strength mechanism is related to atoms in solid solution, precipitates, and grain size [21].
Caceres et al. [75] investigated the influence of Si, Cu, and Mg on the tensile properties of heat-treated Al-Si-Mg-Cu systems. They concluded that to achieve the optimal mechanical response, Cu content should be limited to 3 wt.% when Mg content is above 1 wt.%. Zheng et al. [12] investigated Al-6Si-Cu-Mg alloys with Cu/Mg ratios from 1 to 4. They reported that the precipitation sequence depends on the Cu content and the Cu/Mg ratio: a low-ratio alloy tends to preferentially form the precursor of β precipitates, whereas a high-ratio alloy will lead to the formation of Q and θ precursors.
In cyclic testing, the most straightforward case is loading and unloading the sample in the shape of a sine curve. The parameter settings for the fatigue test are either stress or strain-controlled depending on the test. Preparation for the test parameters depends on the usage of the component in the actual case. The loading route can be different such as low-cycle fatigue (LCF), HCF, very high-cycle fatigue (VHCF), or ultra high-cycle fatigue (UHCF). Fatigue is the localized damage of a component due to repeated loading [4, 76, 77]. Fatigue failure has been a challenge for the industry and researchers to understand since the 15th century. Generally, in HCF loading conditions, up to 90 % of the component fatigue life can be attributed to crack initiation and growth of microstructurally small cracks [4].
When the material is exposed to cyclic loading, its fatigue life is divided into three stages.

(1) The definition of the first initiation point of a fatigue crack can be varying depending on the observer, which can be subjective. The size scale differs from an engineer detecting a crack in mm scale to a material scientist that tries to find the initiation site at a lower microscopic scale. In pure metals, the crack originates from persistent slip bands (PSBs) evolving from cyclic loading because of the irreversibility of the slip planes [78]. In cast Al-Si alloys, the crack initiation originates from local stress concentrations such as surface roughness, defects, intermetallics, etc. Moreover, the as-cast material is more prone to generate slip bands that can act as nucleation sites. Fatigue cracks begin at the regions with the highest stress concentration. Microcracks initially extend along with the slip bands, and the microstructure of the material dominates the early propagation of microcracks [4, 79].

(2) The microstructural aspect of crack propagation is critical for fatigue life, and the scale of the crack is as follows. Moreover, the growth rate of the different cracks is changing during the fatigue life. The separation between the microstructurally, mechanically, and physically short cracks are not evident and commonly gives rise

to confusion. After crack nucleation, the propagation rate is determined by microstructural features such as grain boundaries, precipitates, and pores. The scale of these cracks is termed microstructurally short cracks affected by barriers such as phases, grain boundaries that act as obstacles for the growing crack. The growth rate may accelerate, deaccelerate, and even arrested completely. Once the crack continues to grow and exceeds several grain diameters, the term is mechanically short cracks. The impact of the microstructural features reduces at this stage, and the plastic zone in front of the crack tip dominates the crack propagation. Physically short crack is when the plastic area at the tip is negligible to the crack length, and plasticity crack closure effects may affect the crack growth. Crack growth continues, and intrinsic effect at the crack tip and extrinsic factors such as crack closure occur, and the definition of the crack size is a long crack.

(3) As the propagation continues, gradually reducing the cross-section area of the tested sample. Eventually, the material will weaken, so a final fracture occurs [4].
The material behavior dictates if the crack initiation or the propagation controls the fatigue properties, whereas the initiation dominates in the brittle material, and the propagation is the most govern in a ductile material. The initiation of the crack occurs where the stress concentration is at its maximum, commonly at the surface or the subsurface level. Stress risers may be oxides, porosities, intermetallic phases, notches, or surface roughness [4, 72].
Several authors have investigated the fatigue performance in Al-Si alloys during the last decades. It is well accepted that when defects are present such as porosity and oxides, it affects the fatigue properties. Increasing the amount and size of porosities will significantly decrease fatigue life expectations [80]. Reducing the porosities below a certain critical level will cause the oxides to dominate the fracture behavior [81]. Moreover, decreasing the defects below a level where they have limited impact on the fatigue properties, intrinsic microstructure features in the alloy dictate the fatigue behavior. Certain microstructure features on the fatigue properties are not entirely understood, especially on crack propagation.
Lados et al. [82-85] focused their attention on the influence of microstructural features on short and long fatigue crack growth in heat-treated Al-Si-Mg alloys. They reported that grain size has no significant impact on the fatigue crack growth response, while the crack growth threshold and fracture toughness are influenced by SDAS [82]. In particular, large SDAS materials show high threshold and low fracture toughness. Regarding the α-Al matrix strength, the crack growth rate is higher for T4 samples (low yield strength) than for T6 samples in upper region II and lower region III of the Paris curve. T4 samples show better fatigue crack growth resistance in upper region III due to the ductile tearing in the α-Al matrix [83]. About Si particles, unmodified alloys show superior thresholds compared to the

modified alloys. However, the latter present better fatigue cracks growth characteristics than unmodified alloys in region III, meaning higher toughness [82, 83]. Moreover, contradicting results of a modified A356 alloy with SDAS larger than 60 um showed improved fatigue life with the initiation changed from the porosities to the eutectic regions [86]. Another factor that could influence the fatigue properties is the presence of residual stresses [87]. However, contradicting fatigue crack initiation and propagation results requires an understanding of the complex interaction between α-Al matrix, Si particles, and intermetallic phases. Moreover, the distance between these microstructure features will influence the fatigue crack life and propagation.

1.7 Knowledge gap

The knowledge in the literature about the mechanical performance in Al-Si alloys provides information on the general behavior and the impact of the microstructural features on the crack initiation and propagation. However, there are contradicting results in the literature, and new state-of-the-art tools enable a further investigation to understand the gaps in mechanical performance and fatigue crack initiation and propagation of Al-Si alloys.

One of the drawbacks of cast components is the inhomogenous microstructure and defects that influence the mechanical properties. However, with knowledge about the melt quality, design of castings, mold filling, and solidification could the defect level be limited to an acceptable level. Whereas the role of the intrinsic microstructure features in mechanical properties and fatigue crack initiation and propagation becomes essential.

The fundamental understanding of the microstructural features on crack propagation and fatigue performance is not well understood. The complex interaction between α-Al matrix and intermetallic phases such as Mg- and Cu-rich in different loading conditions is not well established.

In order to develop the knowledge of the complex interaction between the microstructural features, the work involved both laboratory scale and casting in the industry to cover the entire aspect. The addition of Cu to Al-Si alloys increases the mechanical properties, but there are contradicting results in the literature. Moreover, increasing the usage of Al-Si components in critical applications is essential to reduce weight in the automotive industry. This work will provide valuable knowledge that will benefit the design of structural components in vehicles with reduced weight. Moreover, using tools like three-nearest-neighbor (3NN) distance and tortuosity could describe the crack initiation and propagation path, increasing the knowledge to develop high-performance components.

Another way to increase the mechanical performance of an Al-Si-Mg alloy is by applying different post-treatments such as HIP process and heat-treatment. The HIP process may improve the mechanical performance in Al-Si alloys in the HIPped condition compared to the as-cast condition. These expected results are because of the solid solution strengthening occurring in the heat-treatment process. However, there is also contradicting result from the literature showing limited improvement. The variations within a cast component in the as-cast condition in terms of SDAS, porosity, etc., may influence the crack initiation and propagation after exposure to the HIP process and heat-treatment process.

Moreover, the outcome and result of the HIP process in terms of mechanical properties are not thoroughly investigated.

The present study aimed to identify the microstructural features that significantly influence mechanical properties and crack initiation and propagation to provide results that will benefit structural component design in vehicles with reduced weight.

CHAPTER 2

RESEARCH APPROACH

CHAPTER INTRODUCTION

This chapter introduces the purpose and aim of the study and describes the experimental procedure.

2.1 Purpose and aim

This work aims to clarify the effect of microstructural features on the mechanical properties and crack initiation and propagation in Al-Si alloy, focusing on the Cu-rich intermetallics and defects. The aim is to develop knowledge about the strong and weak points in the microstructure of Al-Si alloys that is essential for optimizing alloys toward high-performance alloys. The relation of the microstructural features in different loading conditions affects the initiation and propagation of microstructural cracks. This work results in knowledge in the fatigue area that will benefit the increased usage of optimized Al-Si cast components.

2.1.1 Reflection on the chosen methods

The research method applied in this work is based on experiments using deductive reasoning. The experiments performed on a laboratory-scale are well controlled and evaluated only one parameter at a time. The manufacturing of the investigated samples and the test procedures follows the ISO standards where it is possible. However, sometimes, the lack of material required some modification from the ISO standard. The number of tests in an experiment varies to ensure validity and reliability.

The research plan aims to understand the interaction between the α-Al matrix and different intermetallic phases, defects on the mechanical properties and fatigue crack initiation and propagation. Moreover, it is crucial to understand the fatigue crack growth during different loading conditions such as tensile-compressive, etc. This understanding develops a better knowledge of the mechanical performance of Al-Si alloys.

2.2 Research design

2.2.1 Research perspective

The research is approached from a positivistic perspective using deductive reasoning. This approach is testing a hypothesis by either rejecting or accepting the hypothesis after analyzing the experimental results. The positivistic approach tries to link cause and effect with dependent and independent variables for the experiment. After the experiment with data collection, analysis, and evaluation, the result shows if the hypothesis was falsified or not [88, 89].

2.2.2 Research methodology

The starting point of the research area of interest is to perform research for the scientific and industrial challenges. To better understand the topic of interest, a literature search and gathering information must increase the knowledge in the fatigue area. Moreover, this will find the literature gaps, such as contradiction in results and unexplored or limited research areas, and narrow down the topic to relevant research questions. Experiment to confirm or refute the research questions that are designed. A laboratory experiment is a well-controlled and systematic way of testing variables to verify cause and effect. Industry experiments plan to have a low variation since more personal, environmental, and manufacturing equipment are involved. After an experiment, the analysis of results occurs; these results assist in the discussions to conclude see Figure 6.

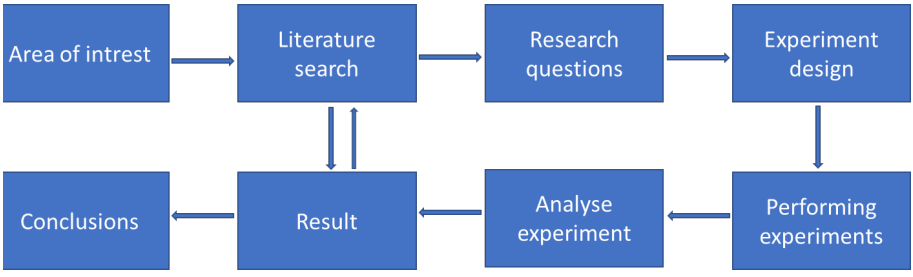

Figure 6. Overview of the research methodology.

In this work, independent variables are intended to be manipulated to study a response. Therefore, the experimental design method is the most suitable for this study.

The research topic was identified considering industrial needs. Subsequently, the literature review reveals the knowledge gaps within the topic, and research questions were formulated. A series of experiments based on the research questions were designed and executed. Through data collection and analysis, conclusions can be stated.

2.2.3 Research questions

The reviewed literature raised questions regarding different microstructural features impact on mechanical properties and fatigue crack initiation and propagation. Furthermore, a discrepancy between different literature results was observed.
The research aims to understand the complicated relationship between the α-Al matrix, and different intermetallic phases and defects on the mechanical properties. This understanding leads to better knowledge in the crack initiation and propagation in the Al-Si alloys with Cu additions. This knowledge leads to the production of optimized components in the automotive industry, resulting in reduced weight and lower emissions. More particularly, this work tries to answer the following research questions.

RQ1 – How will the copper (Cu) affect fatigue crack initiation and propagation in as-cast condition?

The literature reports the general behavior and the role of specific parameters on the fatigue crack initiation and propagation to an Al-Si alloy. However, the addition of Cu in Al-Si alloys is commonly used in the automotive industry to be a competitive component material. This research question tries to answer the influence of Cu addition up to 3.2 wt.% in the as-cast condition. Understanding the complex interaction between Cu in solid solution in the α-Al matrix and the impact of the intermetallic phase in the crack initiation and propagation is addressed. Several techniques have been used to understand what microstructural features influence the crack initiation and propagation; cyclic in-situ testing combined with digital image correlation (DIC) and focus ion beam (FIB) slicing provides unique information. Microstructural observations (e.g., SDAS, grain size, particle size, etc.) increase the understanding of fatigue performance.

RQ2 – How will the heat treatment affect the mechanical properties and fatigue crack initiation and propagation? How will the size, morphology, and distance between the Si and Cu particles affect the performance?

In this research question, the focus is to understand how heat-treatment influences the microstructural feature size and position to each other and how it will affect the propagation of the fatigue crack. The three-nearest-neighbor (3NN) distances will be used to explain the role of the intermetallic phases. Cyclic in-situ testing combined with DIC, Electron backscatter diffraction (EBSD), and FIB slicing provides unique information. This knowledge can be used in component design, alloy development, and/or post solution heat treatment to increase the fatigue life.

RQ3 – How can the variation in size of the porosities within a cast Al-7Si-Mg component exposed to a hot isostatic pressing (HIP) process affect the mechanical properties?

Previous studies in the literature investigate the influence of the HIP process on Al-Si alloys produced with different methods, and the result is difficult to compare. However, the general result is that the HIP process improves the properties. However, within a cast component with different thicknesses, the material properties vary within the component because of; amount and size of porosity, SDAS, and the size of intermetallic phases. The material for this investigation is produced in the industry, and samples are extracted from cast components with different thicknesses. The aim is to understand how the Al-Si alloys microstructure are influenced by the HIP process on the relationship to the fatigue properties. This knowledge will benefit the design of optimized cast Al-Si components for high-performance applications.

2.3 Materials and experimental procedure

2.3.1 Alloys

The base material in the study involved both laboratory scale and casting in the industry to cover the entire aspect. An Al-Si alloy produced from pure material with a variation of the Cu concentration and a commercial Al-Si alloy were investigated.

Table 1. Chemical composition [wt.%] of the investigated alloys, analyzed by OES.

Alloy	Si	Mg	Cu	Fe	Ti	Sr	Na	Al	Alloy designation
EN AC--42000	6.80	0.38	0.00	0.10	0.07	0.03	-	Bal.	Cu 0
EN AC--42000	7.01	0.37	0.51	0.09	0.07	0.02	-	Bal.	Cu 0.5
EN AC--42000	7.14	0.38	1.61	0.09	0.07	0.02	-	Bal.	Cu 1.5
EN AC--42000	6.98	0.36	3.23	0.17	0.08	0.02	-	Bal	Cu 3.0
EN AC-42000 Commersial	7.4	0.36	0.01	0.11	0.13	-	0.01	Bal.	

2.3.2 Casting

Samples were melted in an electrical resistance furnace. Pure Al ingots, pure Si, and an Al-50Mg master alloy were melted in a boron nitride coated crucible to prepare Al-7Si-Mg alloys with different Cu additions. Cu contents were obtained with the addition of an Al-50Cu master alloy. After complete melting, grain refiner (Al-5Ti-1B) and modifier (Al-10Sr) were also added to achieve the targeted contents of 650 - 700 ppm of titanium (Ti) and 200 - 250 ppm of strontium (Sr). Table 1 reports both the name and each alloys chemical composition, the latter evaluated with a Spectromaxx CCD LMXM3 optical emission spectrometer (OES).
Cylindrical rods with a length of 150 mm and a diameter of 9 mm were cast in a preheated graphite-coated permanent mold see Figure 7a. The rods were re-melted and drawn from a Bridgman furnace raising at a ~ 6 mm/s to obtain targeted average SDAS of 10 µm and targeted AGS of 90 µm see Figure 7b. This technique produces a material with a low defect content because the solidification front pushes oxides and porosities towards the top of samples during solidification.

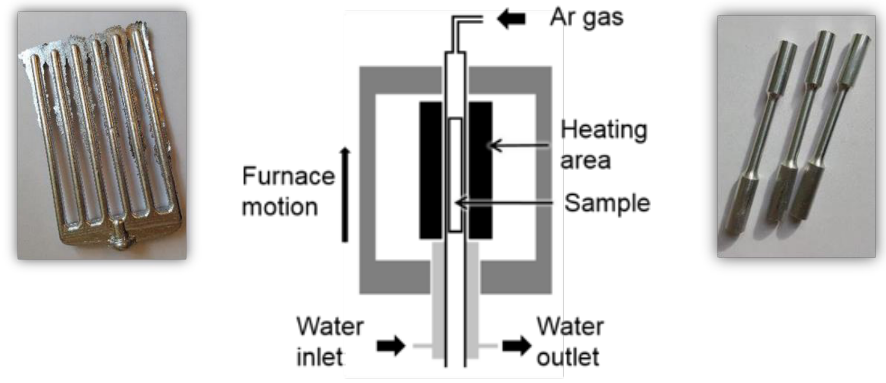

(a) (b) (c)

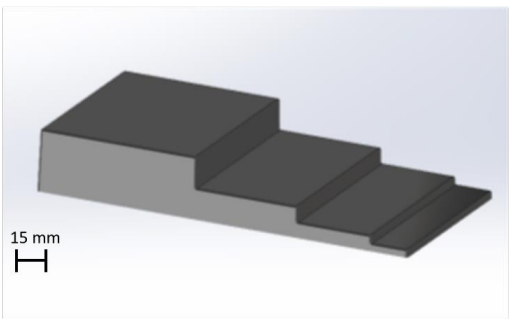

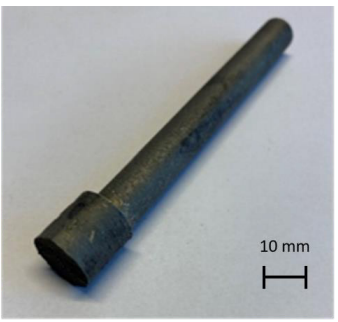

(d) (e)

Figure 7. a) Cylindrical rods (length 150 mm and diameter 9 mm), b) Schematic illustration of the Bridgman furnace, c) Tensile test specimens (length 100 mm, gauge length 36 mm and diameter 6 mm in the gauge length), d) Stair casting geometry, e) Samples for HIP process and heat-treatment.

Samples were cast from a commercial EN AB 42000 alloy in an electric melting furnace. After complete melting, rotary degassing was conducted, grain refiner (Al-5Ti-1B) and modifier Na were added using an automated melt treatment station. The casting was produced in a sand mold in the stair geometry with four different thicknesses, as shown in Figure 7d. Table 1 reports the chemical composition.

2.3.3 Producing samples

Tensile test specimens with a gauge length of 36 mm and a diameter of 6 mm were machined from the staircase castings, and the directionally solidified rods see Figure 7c. Producing miniature compact-tension (CT) samples with an electron discharge machining method using a 0.25 mm wire. The miniature CT sample dimensions, shown in Figure 8a, were designed starting from the ASTM E647-00 Standard guidelines.

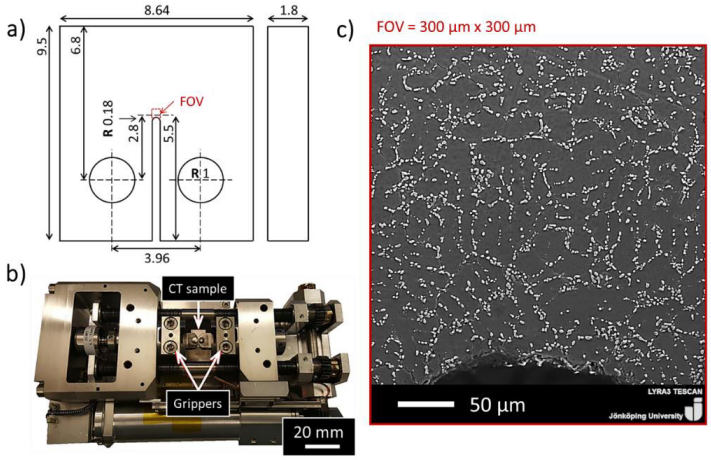

Figure 8 - a) Dimensions of the CT sample in mm; b) miniature stage for in-situ cyclic tests; c) FOV of the CT sample.

Fatigue specimens were machined from the stair casting thicknesses 16 and 32 mm. Samples from the thicknesses were machined to diameter 12 mm and length 100 mm see Figure 7e.

2.3.4 Heat treatment

Solution treatment was performed in an electrical furnace at different temperatures and times for the different studies see Table 2. The time required for heating the samples to the desired temperature was 20 minutes, where excluded from the time presented. The samples were quenched in the water at 50 °C. After the quenching was the samples exposed to naturally aged at room temperature. The artificial aging was performed in an air circulated furnace at different times, and temperatures see Table 2.

Table 2 – Heat-treated cycles for the different investigations.

	Solution temperature °C /time	Natural aging Time	Artificial aging °C/Time
Supplement 2	495 °C /1 h	24 h	210 °C/ 1.5 h
Supplement 3	540 °C /10 h	36 h	170 °C/ 12 h

2.3.5 Hot isostatic pressing

Hot isostatic pressing (HIP) process was carried out to reduce the amount of porosity in specimens. HIP process subjected the specimens to both elevated temperature and isostatic gas pressure in a high-pressure containment vessel. The chamber was heated to a temperature below the solidus temperature but high enough to maximize plastic flow and enhance atom or vacancy diffusion within the specimens. HIP process operating condition was carried out at 540 °C for 2 hours with a pressure of 75 MPa in a high-pressure vessel.

2.4 Microstructure characterisation

2.4.1 Optical microscopy

The microstructure was studied using an optical microscope (Olympus GX71) with image analysis software Stream motion image analyzer and ImageJ. The microstructure features such as SDAS, grain size, particle size, three nearest neighbor distance (3NN), grain size, and tortuosity were measured. The grain size was measured with the linear intercept method as described in ASTM E112-96.
The samples for optical microscopy were prepared with grinding and polishing down to 1μm diamond suspension. The final step was followed by polishing with OP-U suspension. Some samples were etched using a 10% NaOH solution to achieve better contrast.

2.4.2 Scanning electron microscope

The microstructure and fracture surfaces were investigated using a scanning electron microscope (SEM JEOL7001F and Tescan LYRA3). The area fraction of Si particles and intermetallic phases, the distance between particles, length, and

perimeter of particles were measured. The fracture surface of tensile and fatigue samples was investigated.
A JEOL7001F scanning electron microscope equipped with an energy dispersive spectrometer (EDS) was used to analyze the alloys. Mapping of representative areas of the microstructure was carried out to show the distribution of different phases.

2.4.3 Energy-Dispersive X-ray Spectroscopy

Qualitative EDS point analysis was used to measure compositions of intermetallic phases and fracture surface defects. SEM JEOL7001F and Tescan LYRA3 operating at acceleration voltages of 10 and 15kV were used for all the measurements.

2.4.4 Electron Backscattered Diffraction

Electron backscatter diffraction (EBSD) is a technique that provides crystallographic information about the microstructure of a sample. The grain size was determined from the alloys using EBSD on an area of a minimum of 1.5 mm^2. The grains were visualized using inverse pole figure (IPF) maps in the EBSD analysis. The EBSD measurements used an acceleration voltage of 15 kV and a step size of 3 μm. TSL-OIM software was further used to analyze the EBSD maps. The linear intercept method was used to evaluate the AGS. The EBSD maps were acquired before the in-situ test.

2.4.5 Wavelength-Dispersive Spectroscopy

Wavelength dispersion spectroscopy (WDS) is a technique used to measure Mg, Cu, and Si concentrations in the α-Al matrix in the center and the edge of the dendrite. The electron beam penetrates the prepared material and creates vacancies in the atomic shell, which produces x-ray emission detected by the diffractor. The acceleration voltage used was 10kV and 20 kV depending on the measuring element, and for standardization, pure materials of Al, Si, Mg, and Cu were used.

2.4.6 Focused ion beam

Focused ion beam (FIB) milling was applied to produce a random speckle pattern on the in-situ CT samples surface. This was according to the method proposed and validated by Kasvayee et al. [90]. The speckles milled are squares 1 x 1 μm and 1.5 μm depth in an area of 300 x 300 μm at the notch tip producing around 2500 random squares. The surface was etched with NaOH before the milling to maintain a good contrast between the α-Al matrix and the Si particles. FIB milling was used for three-dimensional tomography to observe crack propagation. A location ahead of the propagating crack was selected in an unloaded state, and a rough milling of ~1.7 μA at 30 kV made a trench around the area of interest (AOI). Fine polishing and slicing of the AOI were conducted using a FIB current of ~30 nA at 30 keV. Each slice's thickness was 120 nm and captured around 300 SEM images at 5 keV using a high-sensitivity in-beam Back Scattered Electrons detector.

2.4.7 Digital image correlation

Digital image correlation (DIC) was performed with the commercial software MatchID to determine the strain distribution in the deformed surface. DIC is an optical-numerical measuring technique providing quantitative strains in the field of view (FOV). Table 3 presents the correlation parameters used for the DIC analysis. The size of the FOV was
300 x 300 μm^2, and it comprehended the notch tip to investigate the local strain development. Von Mises equivalent strain, among other strains, is chosen as output. In the DIC software, the subset has square shapes, and the size determines the minimum displacement area. Moreover, the subset (SS) must contain a minimum of three unique features. The correlation occurs by following pixel and the surrounding area in a reference subset-image and deformed subset-image. Step size (ST), the distance between two displacement data points, determines the data of the displacement fields. The strain window (SW) is the number of data points used in the strain calculations. Furthermore, strain spatial resolution (SSR) is limited by the SS and needs to be correlated to the size of the investigate microstructural features. The investigated CT samples need a random pattern, whereas the pattern can follow the surface and detect information from the deformation.

Table 3 - Correlation parameters used for 2D DIC analysis.

	As-cast condition	Heat-treated condition
Pixel size [µm]	0.24	0.24
SS = Subset size [pixel]	61	111
ST = Step size [pixel]	8	11
Correlation criterion	Zero-normalised sum of squared differences	
Shape function	Quadratic	
Interpolation function	Bi-cubic polynomial	
Displacement standard deviation [pixel]	0.1	0.1
SW = Strain window size [pixels]	15	15
SSR = Strain spatial resolution [pixels] SSR = SS + [(SW- 1) · ST]	173	173

2.4.8 Thermo-Calc

The Scheil simulation using the database TCAL2, performed using the Thermo-Calc calculator, enabled to simulate the solidification sequences and to predict the number of different phases in the investigated alloys.

2.5 Mechanical testing

2.5.1 Fatigue testing

Axial fatigue tests were conducted at room temperature for Al-7Si-Mg alloy specimens exposed to the HIP process and heat treatment. The fatigue tests were conducted at a stress ratio of R =-1, using stress-controlled loading at a frequency of 50 Hz in an MTS servo-hydraulic testing machine. Fatigue testing was carried out according to ISO 12107, using the staircase method. The maximum number of cycles was set to 2 x 10^6.

2.5.2 In-situ cyclic testing

In-situ cyclic testing was performed using a miniature loading stage to perform cyclic loading in the LCF range (produced by Kamath & Weiss) see Figure 8b inside an SEM (TESCAN Lyra3) at room temperature. The Field of View (FOV) size was 300 μm x 300 μm, and it comprehended the notch tip to investigate the local strain development (Fig. 8c). The samples were mechanically polished, followed by pattern generation produced either by FIB milling or electropolished (15 V for 5 s) for SEM observations and DIC. EBSD maps were acquired before and after the in-situ fatigue tests to follow the crack propagation and grain boundaries interaction. Before cyclic loading, monotonic tension loading up to failure was performed to select the ΔK. The selected $\Delta K = (1 - R) \cdot K_{max}$ for each alloy, with a constant load ratio R of 0.2. The imposed speed of loading was 8 μm/s (~ 0.1 Hz). The data from the loading stage load (N) and displacement (um) The cyclic testing was stopped at different cycles at maximum and minimum loading conditions to capture high-resolution images for the DIC analysis for the crack initiation and propagation investigation.

2.5.3 Tensile testing

Conventional tensile testing was performed at room temperature, following the SS-EN ISO 6892-1:2016 standard, with a constant cross-head speed of 0.5 mm/min using a Zwick/Roell Z100 equipment equipped with a 100 kN load cell. A minimum of four samples was tested for each condition using a clip-on extensometer with a gauge length of 20 mm to measure the strain. The stress-strain curve data acquired from the system were evaluated to achieve the UTS, YS, and elongation to failure.

2.5.4 Hardness

The hardness of the alloys was measured using a Brinell following the description of the ISO 6506-1:2005 standard, using a 250 kg load and a 5 mm steel ball. Testing was performed at five different locations on each sample from the different thickness of the stair casting.

Nanoindentation testing (100 for each sample) was performed using a Micro materials Nanotest Vantage instrument using a load of 10 mN. The indentation tip was a Berkovitch calibrated using the diamond area function in fused silica material.

Vickers microhardness (HV0.01) testing was performed following the description of the ISO 6507-1:2005 standard.

CHAPTER 3

SUMMARY OF RESULTS AND DISCUSSION

CHAPTER INTRODUCTION

In this chapter, the main results of the appended papers are summarised and discussed. The result and discussion are divided into three major parts to understand the complex interaction between the microstructural features on fatigue crack initiation and propagation.

1) Microstructure investigation, 2) Mechanical properties, and 3) Fatigue crack initiation and propagation.

3.1 MICROSTRUCTURE

3.1.1 Microstructure characterization

The Al-Si-Mg is the base material in this study evaluated with different Cu addition. The microstructure of the as-cast and heat-treated material is shown in Figure 9. The SDAS was measured and, as expected from the cooling rate during directional solidification, results in 9 ± 0.7 μm in all alloys, which corresponds to a cooling rate (CR) of 20 °C/s according to the relation $CR = 48 \cdot SDAS^{-0.4}$ proposed by Samuel and Samuel [23] for Al foundry alloys. The AGS was 95 ± 9 μm, confirming that the alloys were in the same grain refining condition, both in as-cast and heat-treated conditions.

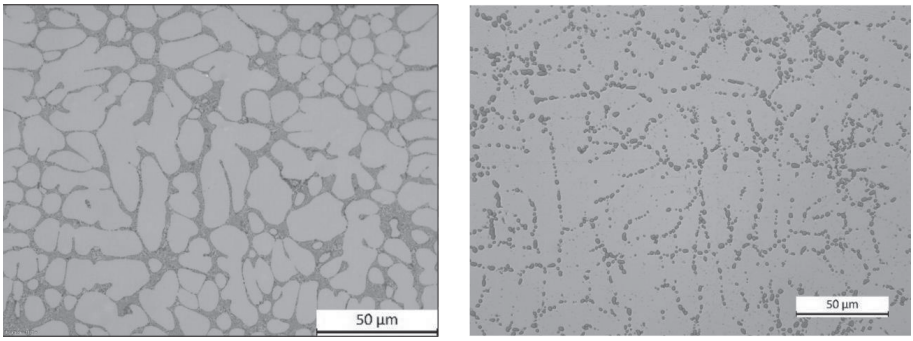

(a) (b)

Figure 9. (a) Alloy Cu 0 in as-cast condition, b) Alloy Cu 0 in the heat-treated condition

The Si particle morphology plays a crucial role on the mechanical properties, from the modified as-cast condition to the solution treatment that spheroidised and coarsened the modified Si particle. Table 4 shows the values of the area and geometrical parameters of Si particles. Aspect ratio ($Feret_{min}$/ $Feret_{max}$) and circularity ($4 \cdot \pi \cdot area/perimeter^2$) are calculated as defined by the ISO 9276-6:2008 Standard. The Si particles area is affected by the heat treatment with an increase, up to 7 times, due to coarsening. However, the aspect ratio and circularity, on the other hand, are not much altered by heat treatment because modified Si particles had a round morphology already in the as-cast condition see Table 4.

Table 4 - Average values and standard deviations of the main results from the investigated alloys.

Alloy	AGS [µm]	SDAS [µm]	Si particles Aspect Ratio	Si particles Area [µm^2]	Si particles Circularity
Cu 0.0	85 ± 5	8.9 ± 0.7	0.57 ± 0.05	042 ± 0.07	0.72 ± 0.05
Cu 0.0 HT	82 ± 4	8.9 ± 0.7	0.63 ± 0.05	1.19 ± 0.53	0.70 ± 0.04
Cu 0.5	85 ± 5	9.0 ± 0.8	0.59 ± 0.05	0.41 ± 0.07	0.74 ± 0.04
Cu 0.5 HT	92 ± 12	8.9 ± 0.7	0.62 ± 0.05	1.49 ± 0.68	0.61 ± 0.03
Cu 1.5	95 ± 9	9.2 ± 0.2	0.58 ± 0.05	0.53 ± 0.09	0.74 ± 0.04
Cu 1.5 HT	107 ± 10	9.2 ± 0.2	0.68 ± 0.05	1.70 ± 0.53	0.74 ± 0.04
Cu 3.0	94 ± 9	8.8 ± 0.1	0.58 ± 0.05	0.44 ± 0.07	0.72 ± 0.05
Cu 3.0 HT	102 ± 9	8.8 ± 0.1	0.81 ± 0.29	1.15 ± 0.69	0.60 ± 0.04

The result from the microstructural investigation in the as-cast condition showed that the presence of Mg leads to the formation of β-Mg_2Si and π-AlFeMgSi phases. As the Cu concentration in the alloy increased to 1.5 wt.%, Mg was involved in π-AlFeMgSi, and Q-$Al_5Mg_8Cu_2Si_6$ phases and θ-Al_2Cu also formed. In Alloy Cu 3.0, the main intermetallic compounds were Q-$Al_5Mg_8Cu_2Si_6$ and θ-Al_2Cu phases. The microstructure investigation agrees with the solidification sequence predicted by the Thermo-Calc simulation software for an Al-Si-Mg alloy with an increasing Cu concentration see Table 5.

Table 5. Solidification sequence of the alloys according to the Scheil simulations with Thermo-Calc.

Solidification reaction	Temperature [°C]			
	Cu 0.0	**Cu 0.5**	**Cu 1.5**	**Cu 3.0**
liq α-Al	616	616	615	608
liq α-Al + Si	573	572	569	565
liq α-Al + Si + Al_5FeSi	566	561	558	551
liq α-Al + Si + Al_5FeSi + $Al_8FeMg_3Si_6$	559	551	528	-
liq α-Al + Si + $Al_8FeMg_3Si_6$ + β-Mg_2Si	557	545	-	-
liq α-Al + Si + $Al_8FeMg_3Si_6$ + β-Mg_2Si + Q-$Al_5Cu_2Mg_8Si_6$	-	530	-	-
liq α-Al + Si + $Al_8FeMg_3Si_6$ + Q-$Al_5Cu_2Mg_8Si_6$	-	-	525	-
liq α-Al + Si + $Al_8FeMg_3Si_6$ + Al_5FeSi + Q-$Al_5Cu_2Mg_8Si_6$	-	520	518	-
liq α-Al + Si + Al_5FeSi + Q-$Al_5Cu_2Mg_8Si_6$	-	-	-	513
liq α-Al + Si + θ-Al_2Cu + Al_5FeSi + Q-$Al_5Cu_2Mg_8Si_6$	-	510	510	510

The microstructure investigated in the as-cast condition is significantly affected by heat treatment. The solution temperature at 495 °C for a time of 1 h dissolved the β-Mg_2Si and most of the Cu-rich phases in the alloys. However, these parameters do not entirely dissolve the Q-$Al_5Mg_8Cu_2Si_6$ phase.

The solidification and heat treatment processes influence the concentration of alloying elements such as Si, Cu, and Mg in the primary α-Al dendrite. Table 6 reports the content of Cu, Si, and Mg obtained from WDS measurements in the α-Al dendrites. In the as-cast condition for all alloys, Si and Mg concentration in the α-Al matrix at the dendrite center resulted in 1.47 ± 0.09 wt.% and 0.03 ± 0.01 wt.%, respectively.

However, the Cu concentration the Alloy Cu 0.5 showed a marginal difference between the center and the edge of the dendrite. For Alloys Cu 1.5 and Cu 3.0, the edge of the dendrite had a slightly higher Cu concentration than the center. The

WDS measurements of Cu, Si, and Mg concentration in the α-Al matrix in as-cast condition agree with previous work by Sjölander and Seifeddine [69].
In the heat-treated alloys, the Cu, Si, and Mg concentration was measured in the α-Al matrix using WDS shown in Table 6. Alloys Cu 0 and Cu 0.5 show Mg and Cu concentrations in the α-Al matrix at the same concentration as measured by the OES, confirming that all Mg_2Si and Cu-based phases dissolve. However, in alloys with a Cu content of 1.5 wt.% and 3 wt.%, traces of the Q-$Al_5Mg_8Cu_2Si_6$ phases formed during solidification is not entirely dissolved. This result is due to the solution treatment performed (495 °C for 1 hour), which does not entirely dissolve the Q phase. The complete dissolution of the Q phases requires either a two-step solution heat treatment presented by Sokolowski et al. [91] and Wang et al. [92] and Toschi [93] or longer than 1 hour. In the heat-treated condition, the concentration of Si and Mg in the center of the primary dendrites showed a slight decrease as the Cu concentration increased: Si from 0.94 ± 0.03 to 0.84 ± 0.01 wt.%, Mg from 0.32 ± 0.01 to 0.27 ± 0.01 wt.% this is because of the not dissolved Q phases, which contains both Si and Mg.

Table 6. Average values and standard deviations of the WDS measurements in primary α-Al.

	Primary α-Al			
Alloy	**Cu [wt.%] centre**	**Cu [wt.%] edge**	**Si [wt.%] centre**	**Mg [wt.%] centre**
Cu 0.0	-	-	1.47 ± 0.09	0.03 ± 0.01
Cu 0.0 HT	-	-	0.94 ± 0.03	0.32 ± 0.01
Cu 0.5	0.11 ± 0.01	0.11 ± 0.02	1.47 ± 0.09	0.03 ± 0.01
Cu 0.5 HT	0.51 ± 0.02	0.50 ± 0.02	0.90 ± 0.02	0.31 ± 0.01
Cu 1.5	0.37 ± 0.03	0.51 ± 0.07	1.47 ± 0.09	0.03 ± 0.01
Cu 1.5 HT	1.42 ± 0.06	1.39 ± 0.05	0.82 ± 0.03	0.31 ± 0.01
Cu 3.0	0.74 ± 0.04	0.90 ± 0.13	1.47 ± 0.09	0.03 ± 0.01
Cu 3.0 HT	2.83 ± 0.09	2.80 ± 0.11	0.84 ± 0.02	0.27 ± 0.02

The area fraction of the Cu phases in the alloy is presented in Table 7. In the as-cast condition were the Q-$Al_5Mg_8Cu_2Si_6$ and θ-Al_2Cu phases coarser than Si particles and confirmed using EDS measurement. Moreover, no θ-Al_2Cu phase in the heat-treated condition was found.

Table 7. Area fraction of the Q phase and θ Phase.

	$Q\text{-}Al_5Mg_8Cu_2Si_6$	θ Phase
Alloy	**Area %**	**Area %**
Cu 0	-	-
Cu 0 HT	-	-
Cu 0.5	0.5	-
Cu 0.5 HT	0.13	-
Cu 1.5	1.4	0.8
Cu 1.5 HT	0.2	-
Cu 3.0	2.2	2.6
Cu 3.0 HT	0.97	-

The heat treatment also influenced the relative distance between the secondary phases in terms of both Si particles and Cu-based compounds. The three-nearest-neighbor (3NN) distance, as developed in [94], of secondary particles (i.e. eutectic Si and Cu phases) was measured using the x and y coordinates of each particle centroid. The FOV in the micrographs constituted the reference system for the coordinates. These 3NN distance measurements are summarised in Figure 10. Si particles (Fig. 10a) present an average 3NN distance of 0.63 μm in as-cast alloys, independent of Cu content. After heat treatment, the distance between the Si particles increased to the range of 1.40 – 2.32 μm due to the coarsening effect. On the other hand, the 3NN distance of Q phases (Fig. 10b) in the as-cast condition decreased from 3.55 μm in Alloy Cu 0.5 to 0.78 μm in Alloy Cu 3.0. This decreasing trend mirrored the increased quantity of intermetallic particles. After heat treatment, the decreasing trend shifted to higher values, from 9.10 μm in Alloy Cu 0.5 to 4.10 μm in Alloy Cu 3.0. (Fig. 10b).

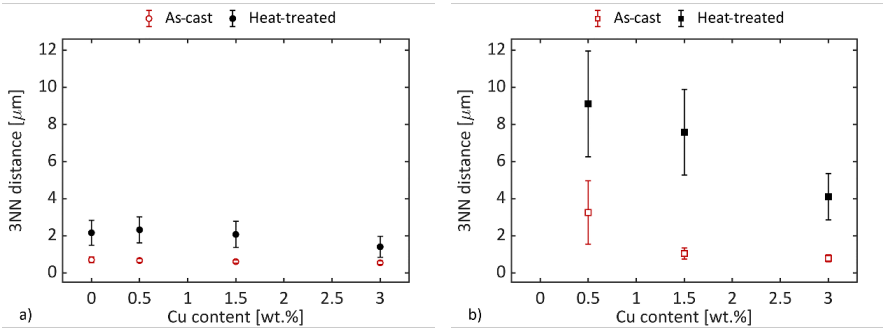

Figure 10 - Three-nearest-neighbour (3NN) distance of particles: a) eutectic Si; b) Q phase. The error bars represent the standard deviation.

Figure 11 illustrates the microstructures of the industrial casted staircase component Al-7Si-Mg alloy in the as-cast condition.

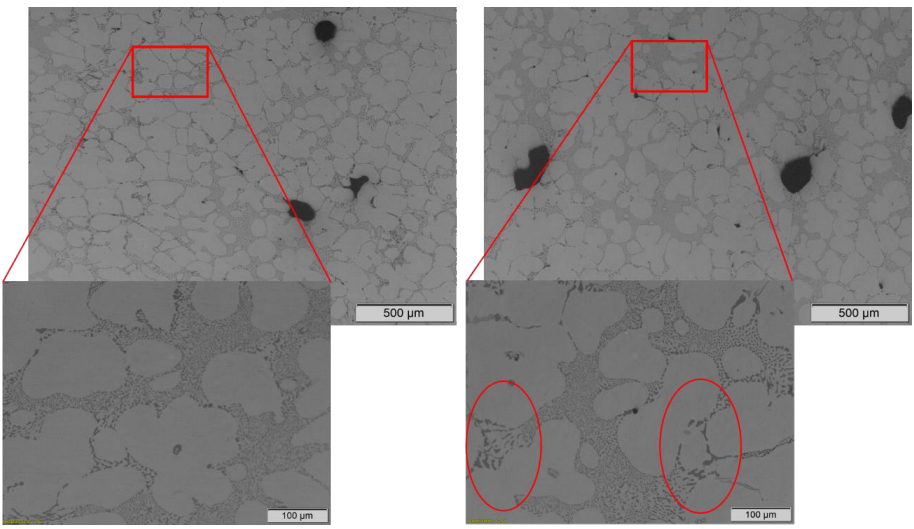

(a) (b)

Figure 11. Microstructures of the Al-7Si-Mg alloy, (a) as-cast condition 16 mm thickness, (b) as-cast condition 32 mm thickness. The red squares highlight a magnified view. The red oval rings highlight the inhomogeneous microstructure in the 32 mm thickness.

The coarser microstructure shows a more inhomogeneous modification level because of the slow cooling rate, even with the recommended addition of Na [95] (highlighted in the magnified picture). The SDAS for the investigated stair

thicknesses 16 mm and 32 mm are 58 ± 6 µm and 81 ± 7 µm. Moreover, a significant difference in porosity size between the two conditions is visible in the micrographs Figure 11, which is also confirmed with the density measurements in Table 8, showing lower density in the coarser microstructure.

The solution treatment parameters are chosen from work by Sjölander et al. [69]. Artificial aging was selected to reach the peak strength of the material. Natural aging of 36 hours before artificial aging was selected, which is beneficial for Al-Si-Mg alloys. It promotes a microstructure with a lower number density of coarser particles than the directly aged material. The chosen artificial aging time of 12 hours was selected from the hardness test of the material exposed for artificial aging at 170 °C in the time interval from time 0 h to 1000 h see Figure 12.

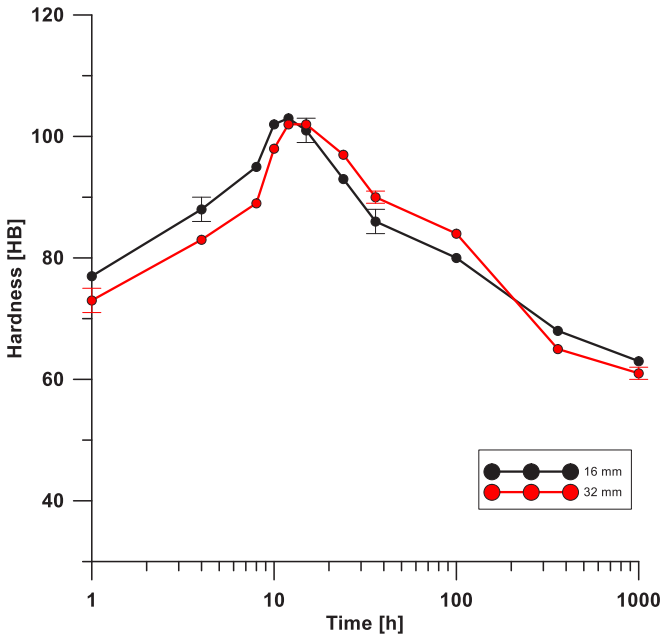

Figure 12. The hardness response of the artificial aging times on the staircase component at 170 °C. The error bars represent the standard deviation.

These hardness values are in line with previous work by Ceschini et al. [62]. In Figure 13, the micrographs of the HIPped and heat-treated material show spherodized and coarsened Si particles and no observed porosities in the different conditions.

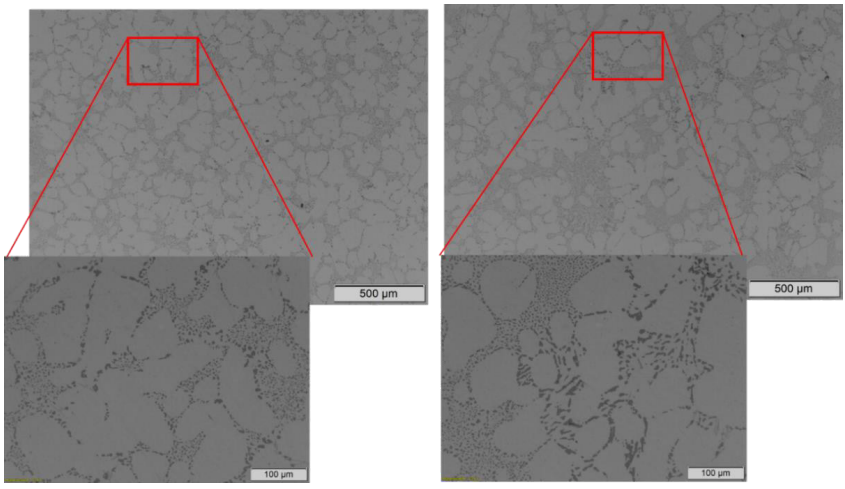

(a) (b)

Figure 13. Microstructures of the Al–7Si-Mg alloy, (a) heat-treated condition 16 mm thickness, (b) heat-treated condition 32 mm thickness. The red squares highlight a magnified view.

Furthermore, the material was exposed to computed tomography scanning in three different conditions: as-cast, after the HIP process, and after heat treatment, shown in Figure 14. The result confirms the observation from the micrographs, whereas the as-cast coarser microstructure contains a higher amount of porosities.

(a) (b)

Figure 14. Computed tomography scanning of the material in as-cast condition showing the porosities (blue), HIPped (red), and heat-treated (green). a) 16 mm, b) 32 mm

The amount of detected porosity in the as-cast condition of the 32 mm thickness shows significantly higher porosity content compared to the 16 mm condition see Table 8, which correlates well with the observation in the micrographs Figure 11. The HIP process impacts are shown in Figure 14, and it still detects porosity larger than the limit of detection (0.25 mm in diameter) in the samples. However, the amount of porosity is close to zero in all HIPped material. After the HIP process, the specimens were exposed to the high solution treatment temperature, which showed no indication that the pores are opening again. These results agree with the HIPped + heat-treated material density measurements equal to the alloys calculated density by Thermo-Calc see Table 8.

Table 8. Average values and standard deviations of the density and computed tomography scanning porosity.

	As-cast 16 mm	**As-cast 32 mm**	**HIPped + T6 16 mm**	**HIPped + T6 32 mm**	**Calculated density by Thermo-Calc**
Density (g/cm^3)	2.655 ± 0.006	2.650 ± 0.007	2.671 ± 0.004	2.670 ± 0.003	2.67
Computed tomography scanning Porosity %	0.05	0.71	0.00	0.00	

The density result and the computed tomography scanning of the as-cast material deviate, indicating that porosity is smaller than the detected limit in computed tomography scanning. Computed tomography scanning, micrographs, and density measurements indicate that the porosities are closed by the HIP process, as reported in the literature [56, 96].

3.2 Static mechanical properties

The mechanical properties are listed in Table 9 are in line with previous results [8-10]: UTS increase up to 1.5 wt.% Cu and elongation continuously decreased. At the same time, YS increased with higher Cu content for the as-cast and heat-treated samples.

Table 9 – Average values and standard deviations of the mechanical properties of the alloys.

Alloy	YS [MPa]	Δ_{YS}	UTS [MPa]	Δ_{UTS}	E [%]	Δ_{E}
Cu 0	107 ± 0.3		255 ± 0.2		19 ± 0.3	
Cu 0.5	117 ± 0.3	+ 9 %	281 ± 2.5	+ 10 %	15 ± 2.2	- 21 %
Cu 1.5	136 ± 0.1	+ 27 %	317 ± 1.0	+ 24 %	14 ± 0.4	- 26 %
Cu 3.0	149 ± 0.2	+ 39 %	252 ± 9.0	- 1.2 %	2 ± 0.3	- 90 %
Cu 0 HT	243 ± 1.1		285 ± 2.5		11 ± 0.5	
Cu 0.5 HT	250 ± 2.9	+ 3 %	317 ± 2.8	+ 11 %	12 ± 0.6	+9%
Cu 1.5 HT	284 ± 1.7	+ 17 %	377 ± 1.7	+ 32 %	11 ± 1.0	0 %
Cu 3.0 HT	327 ± 1.6	+ 35 %	418 ± 2.5	+ 47 %	8 ± 0.5	- 27 %

For the as-cast condition, the increase of YS was comparable to the results reported by Seifeddine et al. [8]. They investigated alloys with chemical compositions, modification treatments, and solidification conditions similar to those described in the present work. Moreover, a remarkable drop in UTS and elongation occurs for the specimen with a Cu content of 3.2 wt.%, whereas other authors reported this reduction at lower Cu contents of around 1.5–2 wt.% [7, 9]. The increased quantity of Q and θ phases in Alloy Cu 3.0 was responsible for reducing UTS and elongation, as highlighted by the analysis of fracture profiles (Fig. 15).

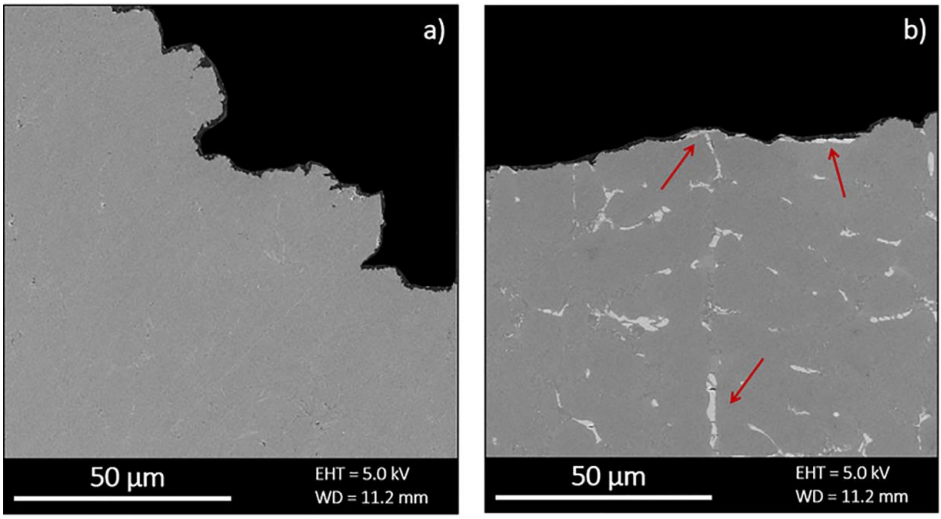

Figure 15. Tensile fracture profiles; a) Alloy Cu 0, b) Alloy Cu 3.0.
Red arrows point at fractured Cu-bearing phases, both on the fracture profile and far from it.

The Q and θ phases change the propagation path from nonlinear in alloy Cu 0 (Fig 15a) to a propagation following intermetallic phases with areas of cleavage behavior in alloy Cu 3.0. Moreover, fractured Cu phases are evident below the fracture profile see Figure 15b. These phase fractures because of the increased strength in the α-Al matrix leading to high stresses in the Cu phases, promoting a rapid propagation.
In the heat-treated condition, the mechanical properties follow the as-cast condition trend with an increase in YS and UTS and a decrease in elongation with increasing Cu concentration, as shown in Table 9. The YS increased from 3 to 35 % as Cu increased from 0.5 to 3.2 wt.%, while UTS increased from 10 to 47 %. However, the reduction in elongation was negligible compared to the reduction in the as-cast material, showing the importance of the detrimental Cu-rich phases. The heat treatment was beneficial, particularly for alloys with Cu contents of greater than 1.5 wt.%, with a limited degree of reduction of the elongation to failure.
The increase in YS and UTS was related to the precipitation hardening in the alloys, reported by Zheng et al. [12]. Comparing the increasing trend of YS and UTS with the WDS measurements (Table 6), it is clear that after heat treatment, the strengthening role of the Cu retained in the primary α-Al matrix was coupled with the partial dissolution of the Q phases and the total dissolution of the θ phases, respectively, during heat treatment. The hardness trend in the primary α-Al matrix correlates well with the YS showing a percentage increase in YS of 34 % from alloy

Cu 0 to alloy Cu 3.0 and the percentage increase in HV0.01 in the primary α-Al matrix was 33 % see Figure 16.

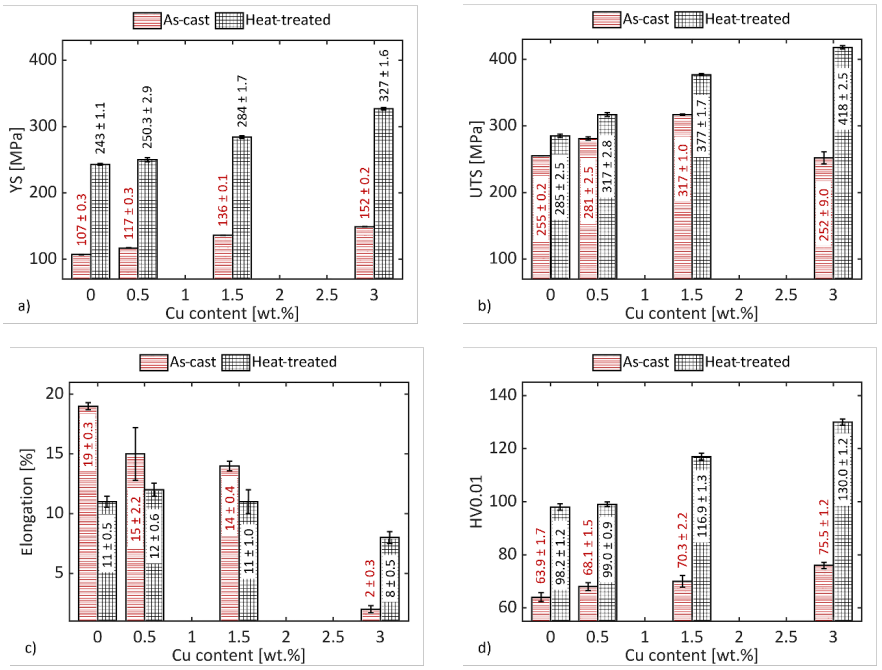

Figure 16 - Comparison of mechanical properties in the as-cast and heat-treated conditions: a) YS; b) UTS; c) percentage elongation; d) Vickers microhardness of the primary α-Al matrix. The error bars represent the standard deviation.

The morphology of the Si particles and the reduced area of intermetallic phases affected the elongation of the material [71]. The limited variation of Si morphology (aspect ratio and circularity in Table. 4) and 3NN distance (Fig. 10a) after heat treatment was common to all alloys and underlined that the mechanical response in this work was primarily affected by the Cu-based phases. The decreasing 3NN distance between Q phases (Fig. 10b) reflected the elongation trends in both conditions. Elongation decreased with Cu content steeply for the as-cast material, from 14 to 2 %, and slightly after heat treatment, from 11 to 8 %. Similarly, the average 3NN distance of the Q phases lay in the 9 – 4 μm range in the heat-treated condition, while in the as-cast condition, the range was 3.5 – 1 μm. The significant drop in elongation in the as-cast condition was due to the reduced distance between

the Cu-rich phases, which cracked and coalesced with neighboring phases leading to a significant elongation reduction.

The industrially cast material was investigated in two different conditions: as-cast and after exposure to the HIP process and heat treatment. The tensile test results in the as-cast condition shown in Table 10 indicate a minor difference in UTS and YS between the two tested conditions. However, a more extensive spread in the elongation to failure is detected in the coarser microstructure, even having samples showing the highest elongation to failure with up to 6 %. This variation could be related to the location of the defects within the samples. These results agree with Riestra et al. [97], which showed a similar improvement of elongation to failure with a modified and grain refined coarser microstructure produced in Bridgman equipment. This equipment shows the possible mechanical properties of an alloy produced with a limited amount of defects. In this case, the larger dendrites are more prone to deform without affecting the surrounding particles.

Results after the HIP process and heat treatment are showing a remarkable difference between the investigated conditions. In contrast, the 16 mm specimen shows an improved elongation to failure from 4 to 6 % and more consistency within the investigated samples. A remarkable decrease in elongation is detected in the 32 mm samples from the as-cast condition 4.6 % ± 1.1 down to 1.1 % ± 0.5. These elongation differences to failure are related to increased α-Al matrix strength, more extensive intermetallic phases, and oxides. Moreover, the closing of the larger porosities by the HIP process influences the elongation to failure because the coarser microstructure is not bonding the oxides inside the porosities completely. The increase of YS and UTS in the HIPped and heat-treated conditions see Table 10 is due to precipitation hardening.

Table 10. Average values and standard deviations of the mechanical properties in the as-cast and HIPped +heat-treated conditions. (fatigue strength was not tested in as-cast condition)

Alloy condition	As-cast		HIPped + heat-treated	
	16 mm	32 mm	16 mm	32 mm
Fatigue strength σ_f (MPa)			142 ± 3.5	127 ± 3.5
UTS (MPa)	159 ± 1.5	148 ± 6.5	315 ± 4	285 ± 11
YS (MPa)	91.2 ± 1.5	91.3 ± 5.7	271 ± 5	261 ± 10
El (%)	4.6 ± 0.4	4.6 ± 1.1	5.9 ± 0.5	1.1 ± 0.5
Ratio UTS/σ_f			0.45	0.44

3.3 Fatigue properties

The HIPped and heat-treated alloys were tested in axial tensile-compression fatigue testing, resulting in fatigue strength of 142 ± 3.5 MPa for the 16 mm thickness. In contrast, the 32 mm showed an 11 % reduced fatigue strength. The ratio between fatigue strength and UTS is in the range reported in the literature [62]. This result indicates that the UTS can be used to evaluate the fatigue strength of the material. Furthermore, the 32 mm samples show a more significant spread in cycles to failure because of the oxide film not eliminated by the HIP process.

3.4 Crack initiation and propagation

The fatigue crack initiation is usually from defects or low surface quality. The in-situ test is a tool to detect the initiation and follow the propagation.

3.4.1 Crack initiation

The fatigue crack initiation in hypoeutectic Al-Si casting alloys usually results from defects at the surface and subsurface levels. However, with a limited number of defects, crack initiation nucleates are generally from discontinuities such as slip bands, particle debonding/breakage, or grain boundaries [98, 99]. In the as-cast alloys is the crack initiation varied depending on the Cu concentration. Preloading did not result in any evident deformation, whereas during cyclic loading, fracture initiation became visible. In alloy Cu 0 and Cu 0.5, slip bands acted as initiation sites. Moreover, in connection with the slip bands, cracking and debonding of Si particles and intermetallics took place, as depicted in the inset of Figure 17a.

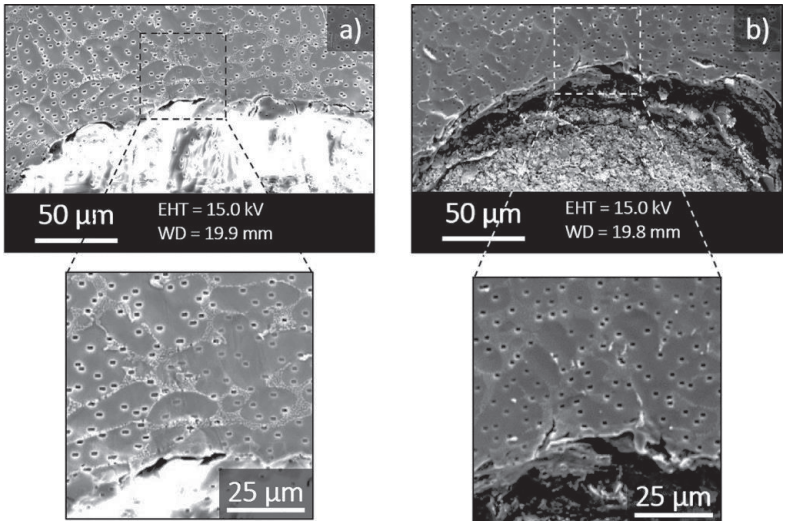

Figure 17. Beginning of crack initiation in as-cast condition: a) Alloy Cu 0; b) Alloy Cu 3.0.

In alloys with 1.5 wt% of Cu content or more, slip bands were not evident as in the other alloys, and fracture nucleated either from the eutectic regions or Cu phases. An example of nucleation in the eutectic region of Alloy Cu 3.0 is depicted in the inset of Figure 17b. This change of the nucleation behavior is linked to strengthening the primary α-Al matrix as Cu increases and crack nucleation moves to the brittle secondary phases in the interdendritic region.

The fatigue crack initiation in heat-treated conditions of a hypoeutectic Al-Si cast alloy showed from a two-dimensional perspective that cracks initiation appeared in the primary dendrite in the Cu-free alloy (Fig. 18a-b). With increasing Cu concentration, it moved to the interdendritic regions (Fig. 18c-h). Figure 18g-h shows that the nucleation sites started at the drawn grain boundaries in Alloy Cu 3.0. Figure 18h shows two cracks that originated from the same point and lie under the black lines representing grain boundaries. On the other hand, Figure 18a-f shows cracks in the center of the grain in all investigated specimens with lower Cu concentrations. From the observation of the polished surfaces, it can be concluded that crack nucleation occurred in the grain for Cu contents up to 1.5 wt.%, and aligned with the grain boundary for Alloy Cu 3.0. Moreover, defects or discontinuities, such as precipitates, can act as initiation sites that were not observed in this work and need different investigative approaches.

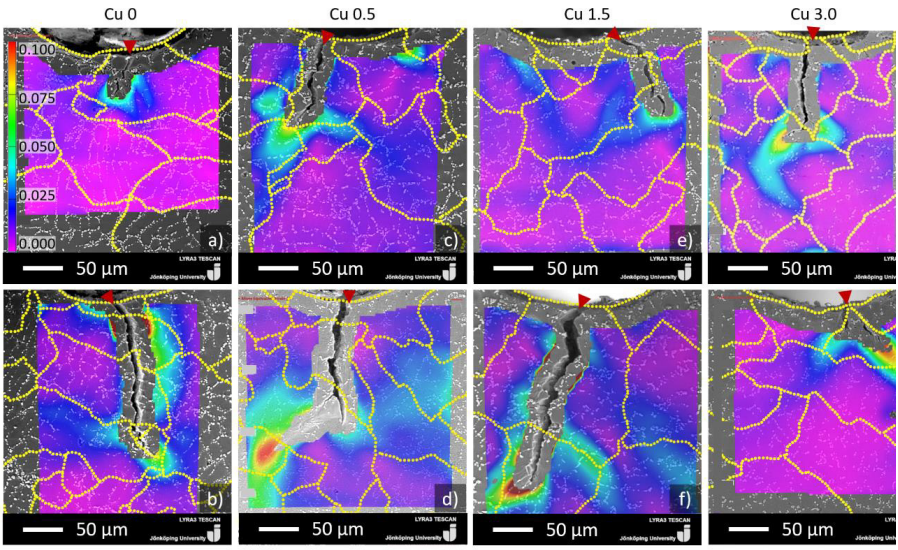

Figure 18. Crack propagation in all heat-treated alloys combining EBSD and DIC: a-b) Alloy Cu 0; c-d) Alloy Cu 0.5; e-f) Alloy Cu 1.5; g-h) Alloy Cu 3.0. The dashed yellow lines represent grain boundaries, superimposed from EBSD, and red arrows point to the initiation sites. The color bar represents the von Mises equivalent strain and is valid for all the frames.

In the industrially cast component exposed to the HIP process and heat-treated, computed tomography scanning showed that all porosities are closed. The fracture surfaces of the fatigue specimen in Figure 19 showed the initiation point with the following propagation zone and a final failure zone. All the fracture surfaces show a mixed mode of ductile fracture and brittle fracture fatigue crack that the cracks initiated near the specimen surface. The 16 mm sample (Fig. 19a) has a significantly larger propagation zone than the 32 mm (Fig. 19b). The fracture surface of the 32 mm samples has a significantly more brittle cleavage area than the 16 mm samples. In the 32 mm samples, these cleavage areas are either Fe-phases or oxides measured with the EDS shown in Figure 20.

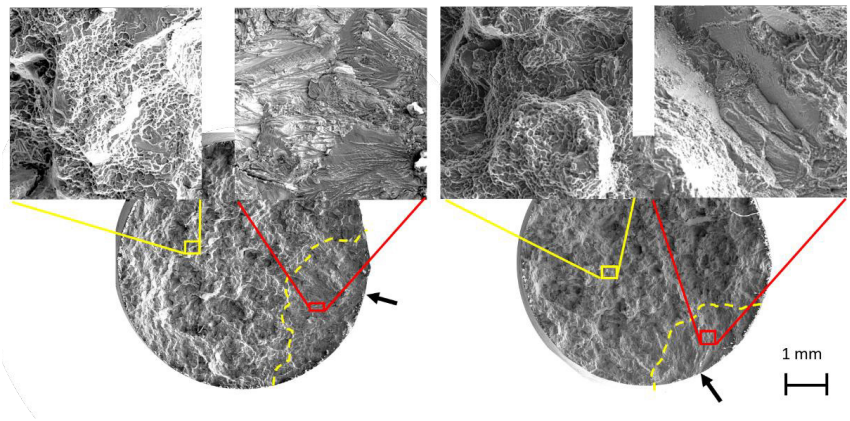

(a) (b)

Figure 19. The fracture surface of the HIPped and heat-treated material. a) 16 mm and b) 32 mm The black arrow shows the initiation sites. The dashed yellow lines show the end of the propagation zone. The red squares highlight the fracture in the propagation zone, and the yellow squares highlight the fracture in the final failure zone.

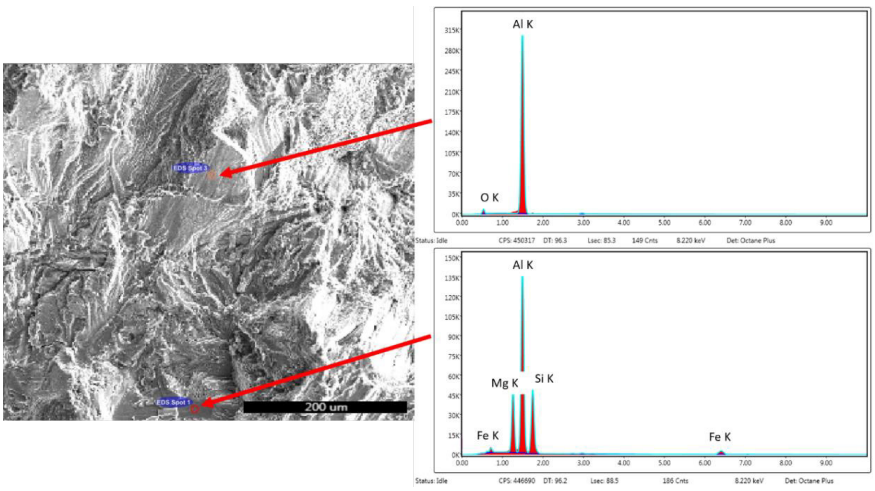

(a) (b)

Figure 20. a) The fracture surface of the 32 mm specimen with two EDS points, b) Related spectrum.

In the in-situ cyclic testing, the HIP process has removed some potential initiation sites. With a limited amount of defects, crack initiation nucleates generally from

surface roughness, discontinuities such as slip bands, or particle debonding/breakage. Figure 21 shows the fatigue crack initiation and propagation of the HIPped and heat-treated CT samples. In the 16 mm samples, after the preload, no visible cracks were observed in the FOV. After 600 cycles, indicate the crack initiation from slip bands at the notch (Fig. 21a). No visible cracks were observed in the 32 mm samples after 300 cycles in the FOV (Fig. 21d). However, at 300 cycles, cracks are opening up in areas away from the notch (Fig. 21e). The orientation of the visible cracks is preferable in the perpendicular direction to the loading.

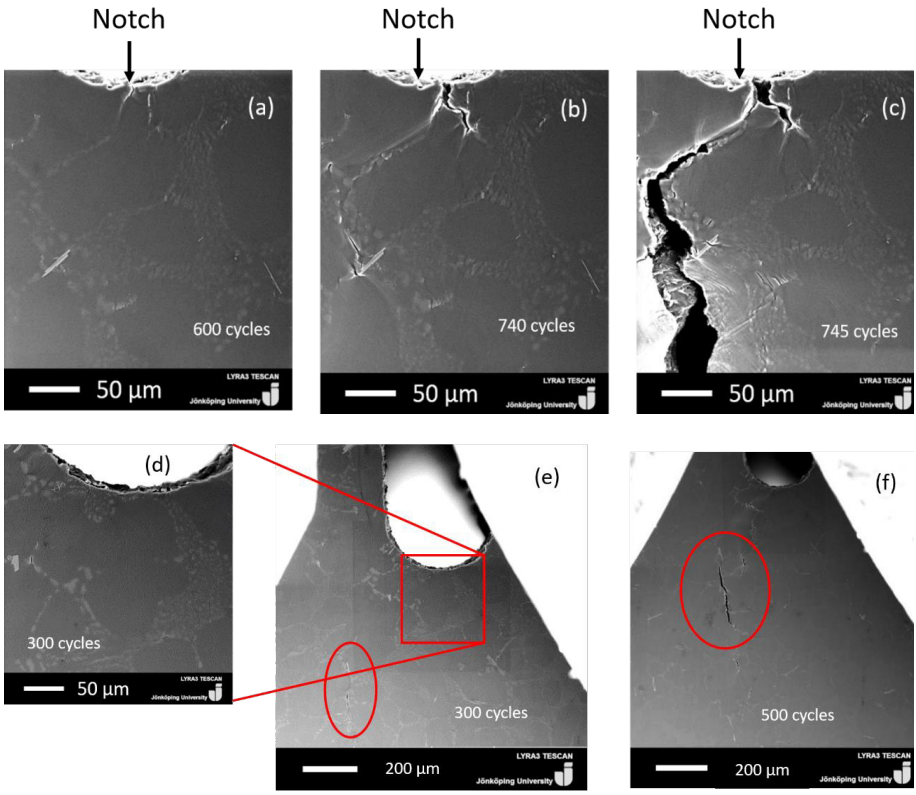

Figure 21. Crack initiation and propagation in the HIPped and heat-treated condition a-c) the 16 mm specimen showing initiation and propagation at the notch of the specimen, d-f) the 32 mm specimen showing cracks and evaluation of crack propagation The red square show an enlarged picture at the notch, and the oval red shape highlights the crack. The circle shape shows the crack propagation after 500 cycles. The white regions in e) and f) are the grippers in the miniature stage.

3.4.2 Crack propagation

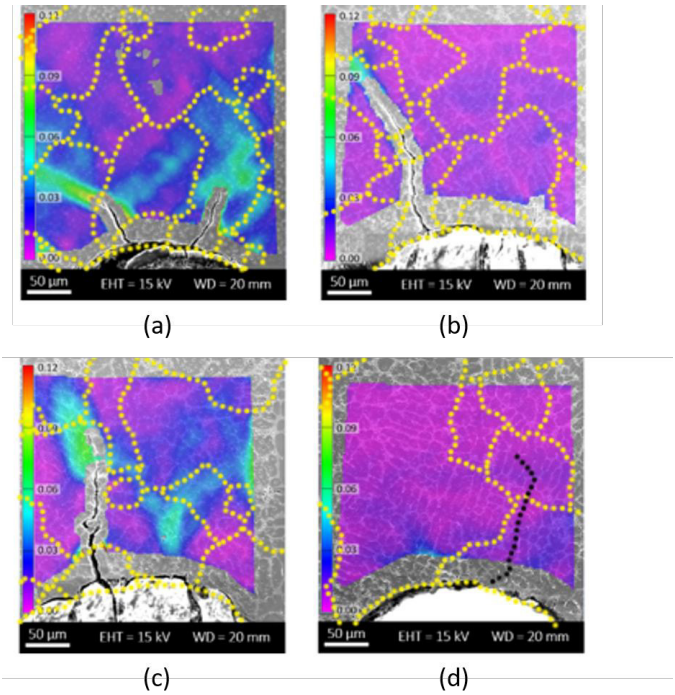

Figure 22. Crack propagation in all as-cast alloys combining EBSD and DIC: a) Alloy Cu 0; b) Alloy Cu 0.5; c) Alloy Cu 1.5; d) Alloy Cu 3.0. The dashed yellow lines represent grain boundaries, superimposed from EBSD. The final fracture is manually drawn with a dashed black line on the picture. The color bar represents the von Mises equivalent strain.

Fatigue cracks are expected to take the path of least resistance, which is generally offered by the most damaged microstructural feature in their path. EBSD orientation maps, acquired to detect grain boundaries before and after failure are highlighted with dashed yellow lines, showed that crack propagation occurred along transgranular paths in all of the as-cast investigated alloys (Fig. 22). In all cases, crack propagation in the FOV was trans-dendritic and crossed the primary α-Al matrix. Figure 22 also depicts that the DIC analysis at 170 N loading enabled highlighting the high-strain (Von mises equivalent strain) regions in alloys with the Cu content up to 1.5 wt%. In most cases, those regions accord well with the crack path of the following cycles.

On the contrary, in Alloy Cu 3.0, the strain was not detected in the FOV before final failure. The fracture path for the first 150 µm in alloy Cu 3.0 was taken from the

final fracture and manually drawn with a dashed black line on the picture. In some other cases, reported in Figure 23 as an example, the DIC analysis results show that the highest strain concentration occurred at the grain boundary. Nonetheless, the crack did not follow that path, and instead propagated across the dendrite arms. Another case show, a local strain concentration in the center of the grain, was evident from DIC, and cracks did not occur nearby (Fig. 23a); later, a crack appeared, most likely coming from the subsurface area (Fig. 23b).

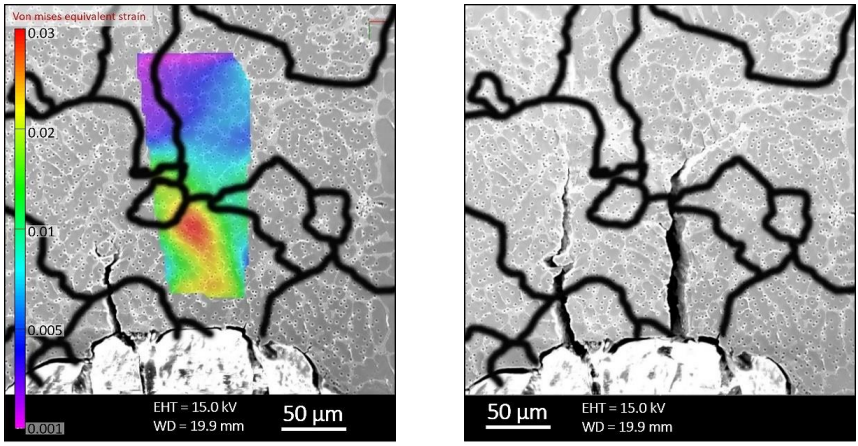

Figure 23. Alloy Cu 1.5. a) After 600 cycles, a high strain area is visible in the area where the crack later propagated; b) After 630 cycles, following crack propagation. The superimposed black lines represent grain boundaries, obtained from EBSD maps.

The DIC can highlight the areas affected by the highest strain in the FOV, but the crack paths do not necessarily correspond to those areas. What is significantly affected by the presence of Cu is the response of the primary α-Al matrix. Figures 24a and b show that in Alloy Cu 0, evident slip bands formed in the dendrite arms throughout the FOV, surrounding the propagating crack during the cyclic test. On the other hand, in Alloy Cu 1.5 slip bands were only visible on the crack edge (Fig.23d) but did not appear in the rest of the FOV (Fig. 23c).

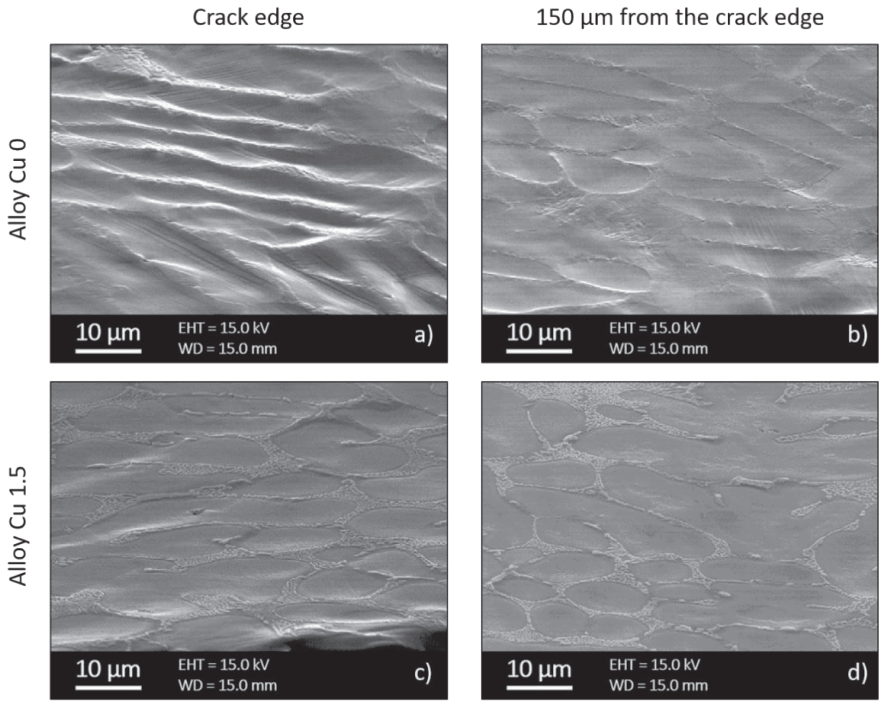

Figure 24. Development of slip bands during the cycling testing of alloys with different Cu contents: a) alloy Cu 0, at the crack edge, b) Cu 0, 150 µm from the crack edge; c) alloy Cu 1.5, at the crack edge, d) Cu 1.5, 150 µm from the crack edge.

The crack path becomes less linear as the Cu content increases. It can be assessed with crack tortuosity, calculated as the ratio between the measured crack length and the equivalent straight path [100]. Given the definition, its values are equal to or higher than 1. In the Alloys, Cu 0 and Cu 0.5 tortuosity is ~1.05, and it increases to 1.2 and 1.3 for Alloys Cu 1.5 and Cu 3.0, respectively. Thus the crack path is influenced by the strengthening of the α-Al matrix and brittle Q and θ phases ahead of the crack tip. With increasing Cu content, the concentration of Cu in the α-Al matrix increased, as shown by WDS analyses (Table 6).

Nevertheless, the crack propagation in all of the alloys followed the α-Al matrix rather than the eutectic regions and grain boundaries in the FOV. The results show that the increased Cu concentration in the α-Al matrix, either in solid solution or fine Cu-rich precipitates, leads to a nonlinear crack propagation path still in the α-Al matrix. In this case, brittle components such as Si particles and Cu phases were expected to behave as a preferential path for crack propagation, but this phenomenon was not observed in the FOV. In the present study, cracks were trans-

dendritic as they propagated along the center of the dendrite or across its arms in the FOV. Moreover, under these conditions, the Cu phases did not affect crack propagation. As a clarifying example of trans-dendritic and trans-granular fracture, Figure 25 shows the crack propagation path and grain boundaries for Alloys Cu 0 (Fig. 25 a) and Cu 0.5 (Fig. 25 b).

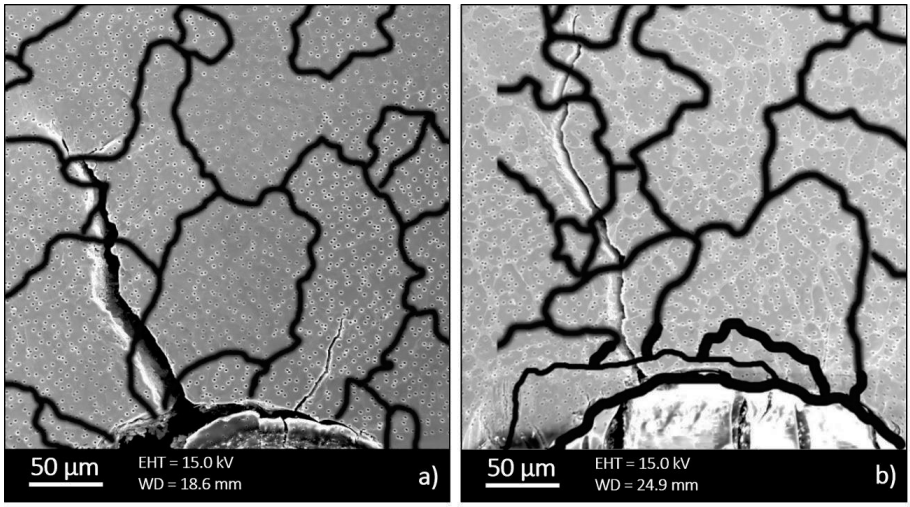

Figure 25. Clear trans-granular crack paths in a) Alloy Cu 0; b) Alloy Cu 0.5. The superimposed black lines represent grain boundaries, obtained from EBSD maps.

Although Cu phases and Si particles are often cracked and debonded from the α-Al matrix, they did not interfere with crack paths. The hardness of eutectic Si is 11.13 ± 0.1 GPa, while that of Q and θ phases is 6.51 ± 1.5 GPa and 5.77 ± 0.7 GPa, respectively, as reported in the literature [101]. A rapid failure occurred in Alloy Cu 3.0 without any previously detectable deformation, so information regarding the crack propagation in the cyclic tests is not available. The increased strength of the α-Al matrix combined with a higher quantity of Cu-rich phases (Table 7) is the reason for the rapid failure. This behavior is similar to that observed in tensile tests of Alloy Cu 3.0, where a sudden drop in elongation to failure occurred despite the increase in YS. Cyclic tests highlighted that the strengthening of the α-Al matrix due to Cu plays a fundamental role in crack nucleation and propagation. The brittle compounds, expected to have a primary role in influencing the alloy's fracture behavior, do not have an evident effect up to 1.5 wt% Cu when the primary α-Al is the constituent that determines the overall response. The EBSD maps generated in the heat-treated alloys were superimposed on the SEM micrograph, and the yellow

dashed lines in Figure 18 represent the grain boundaries. The crack propagation appears to be mixed on the surface, most as trans-granular, and some inter-granular paths were present in all of the alloys.

In Alloy Cu 0 (Fig. 18b), the crack propagated along trans-granular paths for the first 150 μm in the FOV, then continued following the grain boundaries. The propagation followed a mixed path that crossed the dendrite arms and followed the eutectic Si particles.

With the addition of 0.5 wt.% Cu, crack propagation shifted slightly to the interdendritic regions (Fig. 18c-d). This shift occurred due to the increase in α-Al matrix strength due to the retained Cu, evidenced by WDS measurements in Table 6 and hardness values in Figure 16d. The DIC results for Alloy Cu 0.5 highlight that increased strain concentration occurred at the grain boundaries. However, the main propagation path was trans-granular.

In Alloy Cu 1.5 (Fig. 18e-f), the propagation followed the eutectic regions along the dendrite arms, debonding the Si particles from the α-Al matrix. The further strengthening of the primary α-Al matrix in Alloy Cu 1.5 changed the propagation from trans-dendritic to inter-dendritic. The latter is evident for the crack path in Figure 18f. The crack propagated preferentially in the eutectic regions surrounding the α-Al matrix, rather than across the primary dendrites. Despite the increased strain concentration at the grain boundaries, highlighted by DIC in Figure 18f, the propagation remained trans-granular.

About Alloy Cu 3.0 (Fig. 18g-h), the two-dimensional perspective showed that crack growth tended to follow the grain boundaries. Figure 18g shows that the propagation later continued across the grains. In Figure 18h, two cracks, under the dashed yellow lines, are propagated along the grain boundaries and determined the higher strain highlighted by the DIC. The grain boundaries role in these alloys is based on a limited amount of data and needs more investigation. As precipitates, the increased Cu content in the α-Al matrix provides significant obstacles for the dislocation movement, as shown by Roy et al. [102] and Saito et al. [36]. This phenomenon transfers the propagation from the α-Al matrix to the eutectic regions, with an increased number of damaged Si particles and Q phases. Another significant change was the presence of multiple secondary cracks appearing in the FOV during cyclic loading, indicated by arrows in Figure 26.

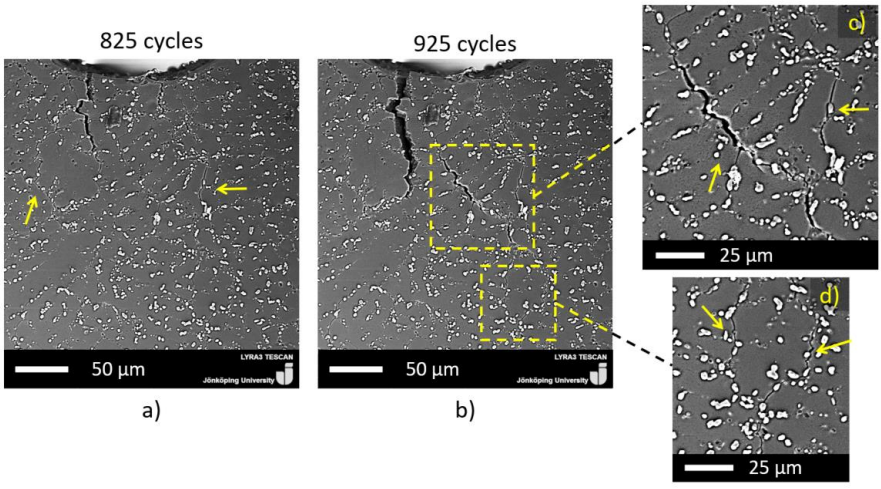

Figure 26. Development of secondary cracks (indicated by arrows) in heat-treated Alloy Cu 3.0: a) 825 cycles; b) 925 cycles; c-d) magnified micrographs of secondary cracks in b).

These secondary cracks followed the Si particles and Q phases (Fig. 26a) and opened up as cyclic loading continued (Fig. 26b). The cracks followed the interdendritic regions and connected the secondary phases due to the reduced 3NN distance between the Q phases, as shown in Figures 26c and d. Secondary cracks were not evident in the FOV of Alloy Cu 0 and Cu 0.5. Moreover, some cracks were detected in Cu 1.5 and increased in the number of secondary cracks in Alloy Cu 3.0. The α-Al matrix strength governed the stress concentrations in the alloy and, consequently, the propagation behavior. Inter-dendritic secondary cracks developed along with the lateral dendrite tips with increasing α-Al matrix strength. The material within the FOV was involved in dissipating the deformation that resulted from the cyclic loading, not only the primary crack but also the secondary cracks in the interdendritic regions.

Lados et al. [103] studied the fatigue crack propagation in T61 and T4 heat-treated A356 alloys, and reported that crack paths changed with increasing ΔK. Cracks propagated in the primary dendrite for ΔK of 5 MPa·√m, and progressively moved towards eutectic interdendritic regions as ΔK increased to 12 MPa·√m. In this study, a similar propagation phenomenon was observed but related to the Cu content of the alloy. In the as-cast condition, Cu shifted the propagation from across the dendrite at low Cu concentrations to the interdendritic regions for Cu contents more significant than 1.5 wt.%. Alloy Cu 3.0 had a rapid failure during the as-cast condition without any previously detectable deformation. However, after the heat

treatment, the crack propagation was not sudden and could be followed in the FOV during in-situ cyclic loadings at all Cu concentration levels. The increased elongation (Fig. 16c) coupled with the increased hardness of the primary α-Al matrix (Fig. 16d) as compared to the as-cast samples highlights the fact that heat treatment of Cu-containing alloys leads to a good balance between strength and ductility. With this condition, the damage is progressive during cyclic loading rather than sudden, as was previously reported for the as-cast condition.
The findings of the secondary cracks in Figure 26 lead to the evaluation using FIB slicing of the extreme conditions, Cu 0 and Cu 3.0.

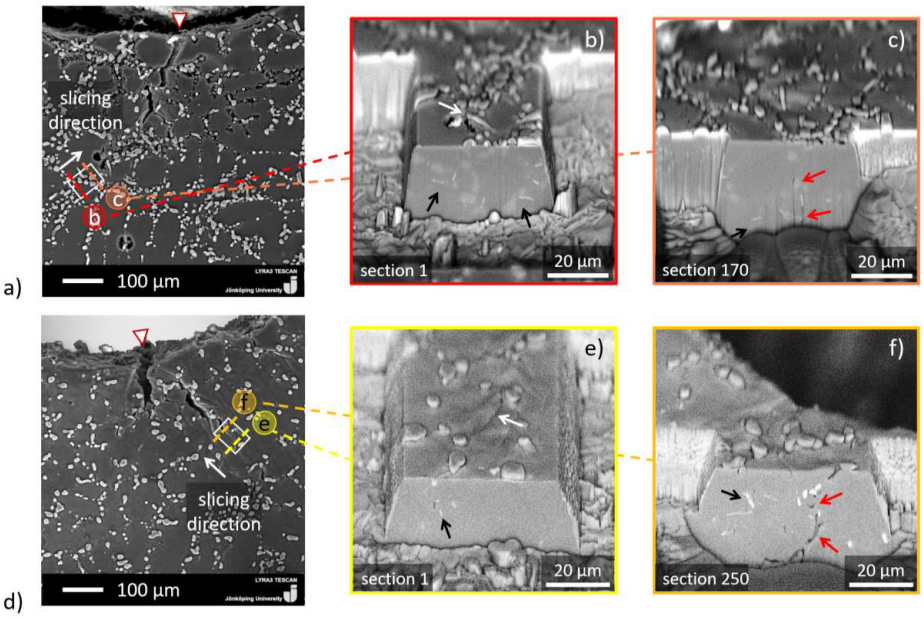

Figure 27. FIB sections were used to investigate the material around the crack in heat-treated alloys. a) Alloy Cu 0, test stopped at 1253 cycles; b) and c) show related sections; d) Alloy Cu 3.0, test stopped at 640 cycles; e) and f) show related sections. The black arrows point to Fe compounds, the white arrows point to superficial cracks, and the red arrows point to the crack coming from underneath.

Figures 27a and d show the AOI (white rectangles) for the FIB sections investigated of Alloy Cu 0 (Fig. 18a) and Cu 3.0 (Fig. 18h). A two-dimensional perspective showed that, during the cyclic testing of Alloy Cu 0, crack propagation stopped at the grain boundary. At the beginning of the FIB sections (Fig. 27b), no crack was visible in the thickness but was evident on the surface (white arrow). The bright

phases in Section 1 (black arrows in Fig. 27b) are Fe-containing phases, as confirmed by EDS measurements. Moreover, investigation of the sections moving toward the crack showed a limited amount of cracked or debonding phases. In Section 170 (Fig. 27c), a crack opened from the underlying volume (red arrows), indicating that crack initiation occurred below the surface.
As the Cu concentration increased to 3.2 wt.% (Fig. 27d), multiple cracks were visible on the surface of the sample. In Figure 27e, the white arrow points to the surface crack, which extends to the material underneath. In the FIB sections, a significant increase in cracked and debonded phases was present ahead of the crack tip as compared to Alloy Cu 0. Moreover, the investigation of the sections moving toward the crack (Section 250 in Fig. 27f) showing crack propagation from below (red arrows) in the intermetallic phases, which were close to each other (~ 4 µm on average, according to the 3NN measurements in Fig. 10b).

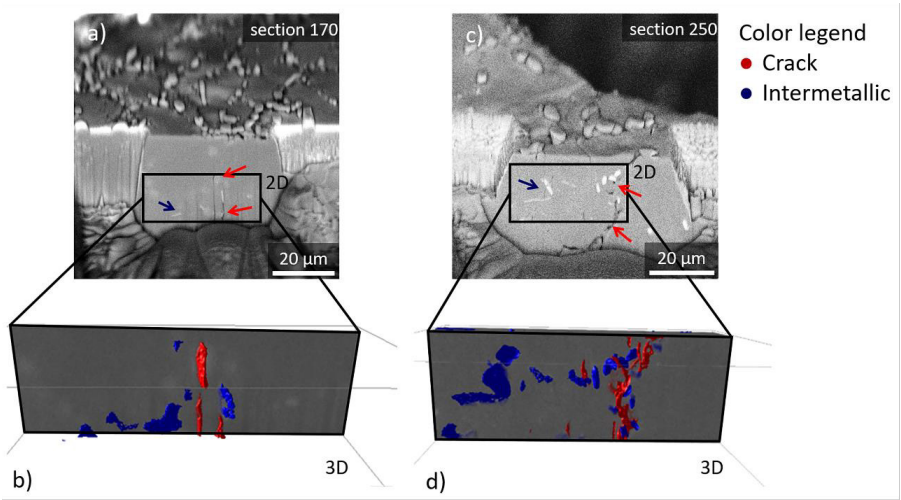

Figure 28 – 3D reconstruction of the FIB sections of the crack in heat-treated alloys. a) FIB section of Alloy Cu 0, test stopped at 1253 cycles, and b) related 3D reconstruction; c) FIB section in Alloy 3.0 Cu, test stopped at 640 cycles, and d) related 3D reconstruction. The red arrows show the cracks, and the blue arrows show the intermetallic phases.

Figure 28 shows the 3d reconstruction of the FIB slicing, showing cracks as red, intermetallic phases as blue in the alloys, whereas the alloy Cu 0 has few cracks in the investigated AOI while Alloy 3.0 Cu contains significant more cracks. In Alloy Cu 0 (Fig 28a), the crack is observed from below, as visualized in section 170 in Fig 27c. In alloy Cu 3.0 (Fig 28b), more microcracks are observed in the AOI, which

are more connected in the FIB slicings start area in section 250. Furthermore, cracks are frequently visible in connection with intermetallic phases, as shown in Fig 27f. These insights regarding crack propagation from subsurface material also apply to the secondary cracks visible in Figure 27. These might be the final parts of cracks that developed underneath due to coalescence between cracked particles that ultimately reached the polished surface and appeared secondary cracks.
The in-situ testing of the industrial cast alloy showed in the 16 mm samples, after 600 cycles, that there is an indication of the crack initiation from slip bands at the notch. At 740 cycles, crack propagation is observed following the eutectic regions and slip bands in the FOV, see Fig 21a. The propagation continues to follow the eutectic regions until failure (Fig. 21c). In the 32 mm specimens, no visible cracks were observed after preloading in the FOV. However, after 300 cycles, a crack opened up in an area away from the notch see Figure 21b. Continued cycling loading to 500 cycles increases the growth of the crack, and an increased amount of crack particles are detected in the FOV (Fig. 21e). However, the large crack that opened away from the notch linked up with the propagation path in the final failure (Fig 21f). This could explain the reduced propagation zone in the fracture surface in Figure 19b. The 32 mm specimen consists of regions, whereas the crack followed the eutectic and cleavage of intermetallics. Moreover, the significant difference in properties between the conditions indicates that the porosity difference before the HIP process affects the propagation path with not healed oxides.

The fracture surfaces of the HCF-tested alloys showed in the 32 mm samples cleavage areas that are either Fe-phases or oxides measured with the EDS shown in Figure 20.
These regions of oxides are the result of closed porosities not healed in the HIP process. Even if the porosity is closed by the HIP process, creating a strong bonding in the oxide film seems complicated. The final failure zone showed a mixed-mode of the ductile and brittle fracture surface.

CHAPTER 4

CONCLUSIONS

CHAPTER INTRODUCTION

In this chapter, the conclusions from the present work are presented.

The present work describes how the complex interaction between specific microstructural features such as Cu-rich intermetallic phases and defects influences the microstructure, mechanical properties, and the fatigue cracks initiation and propagation of an AlSi7Mg alloy. Controlling microstructural features such as SDAS, Si particles, and grain size enabled the focus to be on the impact of Cu intermetallic phases on the mechanical properties and crack initiation and propagation.

The increase of Cu content from 0 wt.% to 3.2 wt.% in the as-cast condition increased the Q-$Al_5Mg_8Cu_2Si_6$ and θ-Al_2Cu phases in Alloy Cu 3.0 to cover an area fraction of 4.8 %.

Concerning mechanical properties in as-cast conditions, an increase in YS of 39% was achieved with the addition of 3.2 wt.% Cu. Moreover, the addition of 1.5 wt.% Cu increased the UTS by 24%. There was, however, a notable reduction of elongation (90%) in Alloy Cu 3.0 because of the reduced 3NN distance between the Cu-rich particles, which was around 1 um, leading to a rapid propagation. The directional solidification did not increase the porosity, proving that the Cu phases are the features that significantly affect the elongation.

In-situ cyclic testing coupled with DIC analysis highlight that the main effect related to Cu addition is the strengthening of the α-Al matrix due to the solid solution in the as-cast condition. This phenomenon significantly changed the alloys response to crack initiation and propagation, in alloys of up to 0.5 wt.% Cu content, slip bands acted as initiation sites; above 1.5 wt% Cu, initiation occurred in the eutectic or intermetallic regions.

Crack propagation appeared to be mixed on the surface, consisting of primarily transgranular propagation in all of the investigated as-cast conditions. However, the crack path moved from trans-dendritic to inter-dendritic as the Cu content in the alloys increased.

The solution temperature at 495 °C for 1 hour dissolved the β-Mg_2Si and most of the Cu-rich phases in the alloys. These parameters do not entirely dissolve the Q-$Al_5Mg_8Cu_2Si_6$ phase. The heat treatment coarsens Si particles and solubilizes

intermetallic compounds. However, the limited variation in terms of Si morphology (aspect ratio and circularity) after heat treatment show that mechanical properties are affected by Cu-based phases to a great extent.
Regarding the mechanical properties in the heat-treated condition, the addition of Cu resulted in a continuous increase in YS and UTS up to 327 MPa and 418 MPa, respectively. The limited percentage elongation decreased from ~ 11 % for Alloys Cu 0 – 1.5 to ~ 8 % for Alloy Cu 3.0. This was because of the reduced number and distance between the Cu-rich phases in Alloy 3.0.
In the heat-treated condition, the most significant microstructural feature affecting crack propagation was the primary α-Al matrix, as the strengthening effect of the Cu influenced the development of interdendritic secondary cracks. In the heat-treated alloy with 3.2 wt.% Cu, the number of cracked particles ahead of the crack tip, and the reduced 3NN distance between the Q phases caused small cracks to coalesce with one another, and these became secondary cracks outside the primary propagation.
The two-dimensional observations provided information regarding crack initiation and propagation that was interpreted differently after the FIB slicing, highlighting a three-dimensional insight into the phenomena. In particular, initiation points in the thicknesses of the CT samples were confirmed by the FIB slicing.

The staircase component shows an inhomogeneous microstructure with different amounts of porosities. The porosity population and coarseness before the HIP process are crucial for the result of the HIP process. The computed tomography scanning results show that all porosities are closed, but the mechanical testing result shows a significant difference between the different thicknesses in the component. This difference in mechanical properties between the conditions indicates that the porosity difference before the HIP process affects the propagation path. The defects not eliminated with the HIP process were detected in the fracture profile, and the fracture surface investigations confirmed that they are detrimental to the mechanical properties.
The coarser microstructure with significantly larger porosities before the HIP process is not healing the oxide surface that has been closed. These oxides assist the crack propagation resulting in reduced mechanical and fatigue properties. The fracture surface contains more and larger cleavage areas in the coarser fracture surface that contain both Fe-rich intermetallics and oxides.
The knowledge added to the science will lead to more designed and optimized structural components and result in lower weight and reduced CO^2 emissions.

CHAPTER 5

FUTURE WORK

CHAPTER INTRODUCTION

In this chapter, ideas based on the current results and findings are presented to continue understanding the fatigue performance to develop high-performance components.

The variation within a cast component depends on the melt quality and the casting process that influences fatigue performance. Producing high-performance components for the critical application requires further knowledge about the microstructural features role in crack propagation. The secondary dendrite arm spacing role is showing contradicting results which is an interesting factor. Moreover, other intermetallic phases such as Fe- phases impact the properties.

Based on the gained knowledge in fatigue crack initiation and propagation in Al-Si alloys, these results could be transferred to other alloy systems such as Al-Mg or Al-Cu. The role of the intermetallic phases formed and the strength of the Al matrix significantly influencing the properties is of interest.

The component in a critical application could be exposed to cyclic loading, which depends on different parameters. The impact on the microstructural features on different loading scenarios such as torsion, bending, rotary bending, and tensile-compression could influence the fatigue properties. It is therefore relevant to evaluate what microstructural phases that are favorable for different loading conditions.

To reach a sustainable society, the recyclability of Al alloys is essential. Usage of secondary Al is degrading the mechanical properties. Furthermore, to what extent could the recycled material be added with limited degradation of mechanical properties in an Al-Si alloy or in an Al wrought alloy.

REFERENCES

[1] A.C. Serrenho, J.B. Norman, J.M. Allwood, The impact of reducing car weight on global emissions: the future fleet in Great Britain, Philosophical Transactions of the Royal Society A: Mathematical, Physical and Engineering Sciences 375(2095) (2017) 20160364.
[2] A.I. Taub, A.A.J.M.B. Luo, Advanced lightweight materials and manufacturing processes for automotive applications, 40(12) (2015) 1045-1054.
[3] E. Balomenos, D. Panias, I.J.M.P. Paspaliaris, E.M. Review, Energy and exergy analysis of the primary aluminum production processes: a review on current and future sustainability, 32(2) (2011) 69-89.
[4] U. Krupp, Fatigue crack propagation in metals and alloys: microstructural aspects and modelling concepts, John Wiley & Sons2007.
[5] I. Serrano-Munoz, J.-Y. Buffiere, C. Verdu, Y. Gaillard, P. Mu, Y. Nadot, Influence of surface and internal casting defects on the fatigue behaviour of A357-T6 cast aluminium alloy, International Journal of Fatigue 82 (2016) 361-370.
[6] C. Nyahumwa, N.R. Green, J. Campbell, The concept of the fatigue potential of cast alloys, Journal of the Mechanical Behavior of Materials 9(4) (1998) 227-236.
[7] R. Taghiabadi, A. Fayegh, A. Pakbin, M. Nazari, M. Ghoncheh, Quality index and hot tearing susceptibility of Al–7Si–0.35 Mg–xCu alloys, Transactions of Nonferrous Metals Society of China 28(7) (2018) 1275-1286.
[8] S. Seifeddine, E. Sjölander, T. Bogdanoff, On the role of copper and cooling rates on the microstructure, defect formations and mechanical properties of Al-Si-Mg alloys, (2013).
[9] S. Shabestari, H. Moemeni, Effect of copper and solidification conditions on the microstructure and mechanical properties of Al–Si–Mg alloys, Journal of Materials Processing Technology 153 (2004) 193-198.
[10] C. Caceres, M. Djurdjevic, T. Stockwell, J. Sokolowski, The effect of Cu content on the level of microporosity in Al-Si-Cu-Mg casting alloys, Scripta Materialia 40(5) (1999) 631-637.
[11] M.T. Di Giovanni, E.A. Mørtsell, T. Saito, S. Akhtar, M. Di Sabatino, Y. Li, E. Cerri, Influence of Cu addition on the heat treatment response of A356 foundry alloy, Materials Today Communications 19 (2019) 342-348.
[12] Y. Zheng, W. Xiao, S. Ge, W. Zhao, S. Hanada, C. Ma, Effects of Cu content and Cu/Mg ratio on the microstructure and mechanical properties of Al–Si–Cu–Mg alloys, Journal of Alloys and Compounds 649 (2015) 291-296.
[13] M. Zamani, S. Seifeddine, A Novel Approach for the Assessment of Eutectic Si Modification and Tensile Properties of Al-Si Cast Alloys, American Foundry Society (AFS) 2015, Design & Production of High Quality Aluminum Castings Conference, Nashville, 5-7 October, 2015, 2015.
[14] I. Polmear, D. StJohn, J.-F. Nie, M. Qian, Light alloys: metallurgy of the light metals, Butterworth-Heinemann2017.
[15] C. Jirang, H.J.J.T.o.N.M.S.o.C. Roven, Recycling of automotive aluminum, 20(11) (2010) 2057-2063.

[16] M. Tiryakioglu, D. Askeland, C. Ramsay, Relationship between metal fluidity and optimum pouring time: a literature review, TRANSACTIONS-AMERICAN FOUNDRYMENS SOCIETY (1993) 685-685.
[17] S. Roy, L.F. Allard, A. Rodriguez, W.D. Porter, A. Shyam, Comparative Evaluation of Cast Aluminum Alloys for Automotive Cylinder Heads: Part II—Mechanical and Thermal Properties, Metallurgical and Materials Transactions A 1-20.
[18] N. Tenekedjiev, J. Gruzleski, Hypereutectic aluminium-silicon casting alloys—a review, Cast Metals 3(2) (1990) 96-105.
[19] O. Atasoy, F. Yilmaz, R. Elliott, Growth structures in aluminium-silicon alloys I. The coupled zone, Journal of crystal growth 66(1) (1984) 137-146.
[20] A. Dahle, K. Nogita, S. McDonald, J. Zindel, L. Hogan, Eutectic nucleation and growth in hypoeutectic Al-Si alloys at different strontium levels, Metallurgical and Materials Transactions A 32(4) (2001) 949-960.
[21] D. Dwivedi, R. Sharma, A. Kumar, Influence of silicon content and heat treatment parameters on mechanical properties of cast Al–Si–Mg alloys, International Journal of Cast Metals Research 19(5) (2006) 275-282.
[22] G. Sigworth, The modification of Al-Si casting alloys: important practical and theoretical aspects, International Journal of Metalcasting 2(2) (2008) 19-40.
[23] A. Samuel, F. Samuel, Effect of alloying elements and dendrite arm spacing on the microstructure and hardness of an Al-Si-Cu-Mg-Fe-Mn (380) aluminium die-casting alloy, Journal of Materials Science 30(7) (1995) 1698-1708.
[24] J.G. Kaufman, E.L. Rooy, Aluminum Alloy Castings, American Foundry Society, Columbus, Ohio (2004).
[25] E. Sjölander, S. Seifeddine, The heat treatment of Al–Si–Cu–Mg casting alloys, Journal of Materials Processing Technology 210(10) (2010) 1249-1259.
[26] A.L. Dons, G. Heiberg, J. Voje, J.S. Mæland, J.O. Løland, A. Prestmo, On the effect of additions of Cu and Mg on the ductility of AlSi foundry alloys cast with a cooling rate of approximately 3K/s, Materials Science and Engineering: A 413 (2005) 561-566.
[27] C. Nayhumwa, N. Green, J. Campbell, Influence of casting technique and hot isostatic pressing on the fatigue of an Al-7Si-Mg alloy, Metallurgical and Materials Transactions A 32(2) (2001) 349-358.
[28] S.J.M.S. Shabestari, E. A, The effect of iron and manganese on the formation of intermetallic compounds in aluminum–silicon alloys, 383(2) (2004) 289-298.
[29] C.M. Dinnis, J.A. Taylor, A.K.J.S.m. Dahle, As-cast morphology of iron-intermetallics in Al–Si foundry alloys, 53(8) (2005) 955-958.
[30] A. Bjurenstedt, S. Seifeddine, A.E. Jarfors, The Effects of Fe-Particles on the Tensile Properties of Al-Si-Cu Alloys, Metals 6(12) (2016) 314.
[31] A. Dahle, K. Nogita, S. McDonald, C. Dinnis, L. Lu, Eutectic modification and microstructure development in Al–Si Alloys, Materials Science and Engineering: A 413 (2005) 243-248.
[32] A. Greer, Overview: Application of heterogeneous nucleation in grain-refining of metals, The Journal of Chemical Physics 145(21) (2016) 211704.
[33] K. Fisher, W. Kurz, Fundamentals of solidification, Trans Tech Publications (1986).

[34] Y. Cho, H.-C. Lee, K. Oh, A. Dahle, Effect of strontium and phosphorus on eutectic Al-Si nucleation and formation of β-Al 5 FeSi in hypoeutectic Al-Si foundry alloys, Metallurgical and Materials Transactions A 39(10) (2008) 2435-2448.
[35] E.A. Mørtsell, F. Qian, C.D. Marioara, Y. Li, Precipitation in an A356 foundry alloy with Cu additions-A transmission electron microscopy study, Journal of Alloys and Compounds 785 (2019) 1106-1114.
[36] T. Saito, E.A. Mørtsell, S. Wenner, C.D. Marioara, S.J. Andersen, J. Friis, K. Matsuda, R. Holmestad, Atomic structures of precipitates in Al–Mg–Si alloys with small additions of other elements, Adv. Eng. Mater. 20(7) (2018) 1800125.
[37] S. Roy, L.F. Allard, A. Rodriguez, T.R. Watkins, A. Shyam, Comparative evaluation of cast aluminum alloys for automotive cylinder heads: part I—microstructure evolution, Metallurgical and Materials Transactions A 48(5) (2017) 2529-2542.
[38] J. Campbell, Castings, Butterworth-Heinemann2003.
[39] D. Dispinar, J. Campbell, Porosity, hydrogen and bifilm content in Al alloy castings, Materials Science and Engineering: A 528(10) (2011) 3860-3865.
[40] D. Dispinar, J. Campbell, Use of bifilm index as an assessment of liquid metal quality, International Journal of Cast Metals Research 19(1) (2006) 5-17.
[41] D. Dispinar, S. Akhtar, A. Nordmark, M. Di Sabatino, L. Arnberg, Degassing, hydrogen and porosity phenomena in A356, Materials Science and Engineering: A 527(16-17) (2010) 3719-3725.
[42] X. Cao, J.J.M. Campbell, M.T. A, The nucleation of Fe-rich phases on oxide films in Al-11.5 Si-0.4 Mg cast alloys, 34(7) (2003) 1409-1420.
[43] M. Tiryakioğlu, The Effect of Hydrogen on Pore Formation in Aluminum Alloy Castings: Myth Versus Reality, Metals 10(3) (2020) 368.
[44] V.-D. Le, N. Saintier, F. Morel, D. Bellett, P. Osmond, Investigation of the effect of porosity on the high cycle fatigue behaviour of cast Al-Si alloy by X-ray micro-tomography, International Journal of Fatigue 106 (2018) 24-37.
[45] P. Osmond, L. Viet-Duc, F. Morel, D. Bellett, N. Saintier, Effect of porosity on the fatigue strength of cast aluminium alloys: from the specimen to the structure, Procedia engineering 213 (2018) 630-643.
[46] J. Linder, M. Axelsson, H. Nilsson, The influence of porosity on the fatigue life for sand and permanent mould cast aluminium, International Journal of Fatigue 28(12) (2006) 1752-1758.
[47] L. Liu, A. Samuel, F. Samuel, H. Doty, S. Valtierra, Influence of oxides on porosity formation in Sr-treated Al-Si casting alloys, Journal of materials science 38(6) (2003) 1255-1267.
[48] A. Samuel, H. Doty, S. Valtierra, F. Samuel, Porosity formation in Al–Si sand mold castings, International Journal of Metalcasting (2017) 1-11.
[49] G.K. Sigworth, T.A. Kuhn, Grain refinement of aluminum casting alloys, International Journal of Metalcasting 1(1) (2007) 31-40.
[50] M. Easton, D.J.M. Stjohn, M.T. A, Grain refinement of aluminum alloys: Part I. the nucleant and solute paradigms—a review of the literature, 30(6) (1999) 1613-1623.

[51] D. StJohn, M. Qian, M. Easton, P. Cao, The Interdependence Theory: The relationship between grain formation and nucleant selection, Acta Materialia 59(12) (2011) 4907-4921.
[52] S.-Z. Lu, A. Hellawell, Growth mechanisms of silicon in Al-Si alloys, Journal of Crystal growth 73(2) (1985) 316-328.
[53] D. Jenkinson, L. Hogan, The modification of aluminium-silicon alloys with strontium, Journal of Crystal Growth 28(2) (1975) 171-187.
[54] M. Timpel, N. Wanderka, R. Schlesiger, T. Yamamoto, N. Lazarev, D. Isheim, G. Schmitz, S. Matsumura, J. Banhart, The role of strontium in modifying aluminium–silicon alloys, Acta Materialia 60(9) (2012) 3920-3928.
[55] A. Knuutinen, K. Nogita, S. McDonald, A. Dahle, Modification of Al–Si alloys with Ba, Ca, Y and Yb, Journal of Light Metals 1(4) (2001) 229-240.
[56] S.J. Mashl, H. Bodycote, Hot Isostatic Pressing of Castings, Casting, 2008.
[57] A. Eklund, M. Ahlfors, Heat treatment of PM parts by Hot Isostatic Pressing, Metal Powder Report 73(3) (2018) 163-169.
[58] H. Atkinson, S. Davies, Fundamental aspects of hot isostatic pressing: an overview, Metallurgical and Materials Transactions A 31(12) (2000) 2981-3000.
[59] I. Radomir, V. Geamăn, M. Stoicănescu, Densification mechanisms made during creep techniques applied to the hot isostatic pressing, Procedia-Social and Behavioral Sciences 62 (2012) 779-782.
[60] C. Lei, W. Frazier, E. Lee, The effect of hot isostatic pressing on cast aluminum, Jom 49(11) (1997) 38-39.
[61] G. Ran, J. Zhou, Q. Wang, The effect of hot isostatic pressing on the microstructure and tensile properties of an unmodified A356-T6 cast aluminum alloy, Journal of alloys and compounds 421(1-2) (2006) 80-86.
[62] L. Ceschini, A. Morri, G. Sambogna, The effect of hot isostatic pressing on the fatigue behaviour of sand-cast A356-T6 and A204-T6 aluminum alloys, Journal of materials processing technology 204(1-3) (2008) 231-238.
[63] M. Brummer, H. Hoffmann, E. Werner, J. Yokohama, S. Kumai, Heat treatment of aluminum castings combined with hot isostatic pressing, Proc. 12th Int. Conf. on Aluminum Alloys, 2010.
[64] T. Rich, J. Orbison, R. Duncan, P. Olivero, R. Peterec, The effect of hot isostatic pressing on crack initiation, fatigue, and mechanical properties of two cast aluminum alloys, Journal of materials engineering and performance 8(3) (1999) 315-324.
[65] D. Apelian, S. Shivkumar, G. Sigworth, Fundamental aspects of heat treatment of cast Al-Si-Mg alloys, AFS transactions 97 (1989) 727-742.
[66] S. Beroual, Z. Boumerzoug, P. Paillard, Y. Borjon-Piron, Effects of heat treatments and minor addition of small amounts of Cu and Mg on the microstructure and mechanical properties of Al-Si-Cu and Al-Si-Mg cast alloys, Journal of Alloys and Compounds (2018).
[67] J.M. Boileau, J.E. Allison, The effect of solidification time and heat treatment on the fatigue properties of a cast 319 aluminum alloy, Metallurgical and materials transactions A 34(9) (2003) 1807-1820.

[68] A. Mohamed, F. Samuel, Influence of Mg and solution heat treatment on the occurrence of incipient melting in Al–Si–Cu–Mg cast alloys, Materials Science and Engineering: A 543 (2012) 22-34.
[69] E. Sjölander, S. Seifeddine, Optimization of solution treatment of cast Al-7Si-0.3 Mg and Al-8Si-3Cu-0.5 Mg alloys, Metallurgical and Materials Transactions A 45(4) (2014) 1916-1927.
[70] L. Pedersen, L. Arnberg, The effect of solution heat treatment and quenching rates on mechanical properties and microstructures in AlSiMg foundry alloys, Metallurgical and Materials Transactions A 32(3) (2001) 525-532.
[71] S. Roy, L.F. Allard, A. Rodriguez, W.D. Porter, A. Shyam, Comparative evaluation of cast aluminum alloys for automotive cylinder heads: Part II—mechanical and thermal properties, Metallurgical and Materials Transactions A 48(5) (2017) 2543-2562.
[72] N.E. Dowling, Mechanical behavior of materials: engineering methods for deformation, fracture, and fatigue, Pearson2012.
[73] T. Bogdanoff, S. Seifeddine, A.K. Dahle, The effect of SI content on microstructure and mechanical properties of Al-Si alloy, La Metallurgia Italiana 108(6) (2016).
[74] E. Ghassemali, M. Riestra, T. Bogdanoff, B.S. Kumar, S. Seifeddine, Hall-Petch equation in a hypoeutectic Al-Si cast alloy: grain size vs. secondary dendrite arm spacing, Procedia Engineering 207 (2017) 19-24.
[75] C. Caceres, I.L. Svensson, J. Taylor, Strength-ductility behaviour of Al-Si-Cu-Mg casting alloys in T6 temper, International Journal of Cast Metals Research 15(5) (2003) 531-543.
[76] U. Krupp, A. Giertler, S. Siegfanz, W. Michels, Mutual Interaction between Fatigue Crack Initiation/Propagation and Microstructural Features in Cast Aluminum Alloys, Advanced Materials Research, Trans Tech Publ, 2014, pp. 488-493.
[77] K.S. Chan, Roles of microstructure in fatigue crack initiation, International Journal of Fatigue 32(9) (2010) 1428-1447.
[78] S. Suresh, Fatigue of materials, Cambridge university press1998.
[79] Q. Wang, D. Apelian, D. Lados, Fatigue behavior of A356-T6 aluminum cast alloys. Part I. Effect of casting defects, Journal of Light Metals 1(1) (2001) 73-84.
[80] M. Leitner, C. Garb, H. Remes, M. Stoschka, Microporosity and statistical size effect on the fatigue strength of cast aluminium alloys EN AC-45500 and 46200, Materials Science and Engineering: A 707 (2017) 567-575.
[81] C. Chama, Elimination of porosity from aluminum-silicon castings by hot isostatic pressing, Journal of Materials Engineering and Performance 1(6) (1992) 773-779.
[82] D.A. Lados, D. Apelian, Fatigue crack growth characteristics in cast Al–Si–Mg alloys: Part I. Effect of processing conditions and microstructure, Materials Science and Engineering: A 385(1-2) (2004) 200-211.
[83] D.A. Lados, D. Apelian, J.F. Major, Fatigue crack growth mechanisms at the microstructure scale in Al-Si-Mg cast alloys: Mechanisms in regions II and III, Metallurgical and Materials Transactions A 37(8) (2006) 2405-2418.

[84] A.G. Spangenberger, X. Chen, D.A.J.M. Lados, M.T. B, Processing Parameter Control of Lifetime-Limiting Failure Mechanisms in Al-Si Cast Alloys at Room and Elevated Temperatures, 49(5) (2018) 2133-2144.
[85] D.A. Lados, D. Apelian, L. Wang, Solution treatment effects on microstructure and mechanical properties of Al-(1 to 13 pct) Si-Mg cast alloys, Metallurgical and Materials Transactions B 42(1) (2011) 171-180.
[86] Q. Wang, D. Apelian, D. Lados, Fatigue behavior of A356/357 aluminum cast alloys. Part II–Effect of microstructural constituents, Journal of light metals 1(1) (2001) 85-97.
[87] D.A. Lados, D. Apelian, The effect of residual stress on the fatigue crack growth behavior of Al-Si-Mg cast alloys—mechanisms and corrective mathematical models, Metallurgical and Materials Transactions A 37(1) (2006) 133-145.
[88] K. Williamson, Research methods for students, academics and professionals: Information management and systems, Elsevier2002.
[89] P. Johannesson, E. Perjons, An introduction to design science, Springer2014.
[90] K.A. Kasvayee, E. Ghassemali, K. Salomonsson, S. Sujakhu, S. Castagne, A.E. Jarfors, Microstructural strain mapping during in-situ cyclic testing of ductile iron, Materials Characterization 140 (2018) 333-339.
[91] J.H. Sokolowski, X. Sun, G. Byczynski, D. Northwood, D. Penrod, R. Thomas, A. Esseltine, The removal of copper-phase segregation and the subsequent improvement in mechanical properties of cast 319 aluminium alloys by a two-stage solution heat treatment, Journal of Materials Processing Technology 53(1-2) (1995) 385-392.
[92] G. Wang, Q. Sun, L. Feng, L. Hui, C. Jing, Influence of Cu content on ageing behavior of AlSiMgCu cast alloys, Materials & design 28(3) (2007) 1001-1005.
[93] S. Toschi, Optimization of A354 Al-Si-Cu-Mg Alloy Heat Treatment: Effect on Microstructure, Hardness, and Tensile Properties of Peak Aged and Overaged Alloy, Metals 8(11) (2018) 961.
[94] J.J. Friel, Practical guide to image analysis, ASM international2000.
[95] N. Rathod, J. Manghani, Effect of modifier and grain refiner on cast Al-7Si aluminum alloy: A review, International Journal of emerging trends in engineering and development 5(2) (2012) 574-582.
[96] J.T. Staley Jr, M. Tiryakioğlu, J. Campbell, The effect of hot isostatic pressing (HIP) on the fatigue life of A206-T71 aluminum castings, Materials Science and Engineering: A 465(1-2) (2007) 136-145.
[97] M. Riestra, E. Ghassemali, T. Bogdanoff, S. Seifeddine, Interactive effects of grain refinement, eutectic modification and solidification rate on tensile properties of Al-10Si alloy, Materials Science and Engineering: A 703 (2017) 270-279.
[98] L. Ceschini, A. Morri, S. Toschi, S. Seifeddine, Room and high temperature fatigue behaviour of the A354 and C355 (Al–Si–Cu–Mg) alloys: Role of microstructure and heat treatment, Materials Science and Engineering: A 653 (2016) 129-138.
[99] K. Gall, N. Yang, M. Horstemeyer, D.L. McDowell, J. Fan, The debonding and fracture of Si particles during the fatigue of a cast Al-Si alloy, Metallurgical and Materials Transactions A 30(12) (1999) 3079-3088.

[100] J.-M. Song, C.-F. Huang, H.-Y. Chuang, Microstructural characteristics and vibration fracture properties of Sn-Ag-Cu-TM (TM= Co, Ni, and Zn) alloys, Journal of electronic materials 35(12) (2006) 2154-2163.
[101] C.-L. Chen, A. Richter, R.J.I. Thomson, Investigation of mechanical properties of intermetallic phases in multi-component Al–Si alloys using hot-stage nanoindentation, 18(4) (2010) 499-508.
[102] S. Roy, L.F. Allard, A. Rodriguez, T.R. Watkins, A. Shyam, Comparative Evaluation of Cast Aluminum Alloys for Automotive Cylinder Heads: Part I—Microstructure Evolution, Metallurgical and Materials Transactions A (2017) 1-14.
[103] D.A. Lados, D. Apelian, P.E. Jones, J.F. Major, Microstructural mechanisms controlling fatigue crack growth in Al–Si–Mg cast alloys, Materials Science and Engineering: A 468 (2007) 237-245.

The Influence of Microstructure on the Crack Initiation and Propagation in Al-Si Casting Alloys

The need to produce lighter components in the automotive industry and especially in electric vehicles is an opportunity and challenge for aluminum-silicon (Al-Si) alloys. These alloys have a high strength-to-weight ratio, high thermal conductivity, good corrosion resistance, good castability, and recyclable and attractive competitors to steel, cast iron, and titanium component. The challenge is to produce a high-performance Al-Si component where several parameters influence the final performance, such as melt quality, alloy composition, casting process, post-treatments, etc. This thesis focuses on the mechanical performance of Al-Si alloys with addresses key microstructural features in the alloys. Understanding the relationship between these microstructural features in the Al-Si alloys widens the usage of high-performance Al-Si alloys. These results will provide guidelines for optimizing the performance in Al-Si alloys both in the component design, alloy composition, and post-treatment.

The amount of Cu retained in the α-Al matrix in as-cast and heat-treated conditions significantly influenced the static mechanical properties by increasing yield strength and ultimate tensile strength with a decrease in elongation. In the as-cast condition, the relation between the addition of Cu and mechanical properties showed that the Cu-rich intermetallic phases formed with the addition of Cu up to 1.5 wt.% did not affect the fatigue behavior, and the crack propagation in these cases was trans-granular and trans-dendritic. The results showed that strain accumulation was highest at the grain boundaries; however, the crack preferred to propagate along or across the primary α-Al matrix due to the relatively lower mechanical strength of the α-Al-matrix compared to the eutectic and intermetallic phases. Moreover, the addition of Cu of more than 3.0 wt.% to Al-Si-Mg alloys changes the fatigue behavior leading to a rapid failure.

The heat-treatment in the Cu added alloys dissolves most of the Cu-rich phases, increasing mechanical properties. This reduction of detrimental Cu-rich phases shows a remarkable improvement in elongation to failure than the as-cast condition.

The hot isostatic pressing (HIP) process is a tool to reduce the internal porosities within a cast component. The findings in this work show that porosity in the as-cast condition influences properties and crack initiation and propagation after the HIP process. The findings show a significant reduction with a coarser microstructure.

The present study aims to identify the microstructural features that significantly influence the mechanical performance of the Al-Si alloy. These results are beneficial for the design of optimized structural components.

TONI BOGDANOFF is currently a Ph.D. student in the Department of Material and Manufacturing at the School of Engineering, Jönköping University. He holds a M.Sc. degree in Product development, specialization in Materials and Manufacturing at Jönköping University. The research interests lie in the field of materials science and engineering and mechanical properties of metallic materials.

ISBN 978-91-87289-66-8